Computing of Lubricant Film Thickness in Cold Rolling Process

Sadiq Muhsin Ihmood

Mechanical Engineering Department

College of Engineering
Thi-Qar University
sadiqmuhsin@yahoo.com

Abstract

The aim of this work is to study the effect of the following parameters :reduction in thickness , length of contact, rolling radius, viscosity of lubricant oil, and roll speed on the lubricant film thickness which are pointed to as an independent variables. In order to illustrate the effect of these parameters, three types of lubricants ,A(Commercial rolling oil, known as Roll oil 981), B (Forming cutting oil called Exx cut 225, with additive) and C (Forming cutting oil called Exx cut 225). Were selected also three values for roll radius (55,65,and 75 mm), with three values for roll velocities (0.5, 1, and 1.5 m/s), and finally five values for reduction in thickness (75, 80, 85, 90, and 95%) were examined to cover all inquires in this work.

The study shown that an increase in roll radius leads to increase in lubricant film thickness . At high reduction, the lubricant film thickness becomes very small, and requires the use of high viscosity lubricant.

Keywords : Cold rolling ; lubricant film thickness**.**

<div dir="rtl">

حساب سمك طبقة سائل التزييت في عملية الدرفلة على البارد

المستخلص

الهدف من هذا البحث هو لدراسة تأثير المتغيرات الاتية : التخفيض في السمك, طول التلامس, نصف قطر الدرفيل, لزوجة سائل التزييت, وسرعة الدرفيل على سمك طبقة سائل التزييت والتي يشار إليها بأنها عوامل غير معتمدة.ولكي نوضح تأثير هذه المتغيرات, تم اخذ ثلاثة أنواع من سوائل التزييت (Roll oil 981), (Exx cut 225, with additive) و (Exx cut 225), كذلك ثلاث قيم من نصف قطر الدرفيل(55,65, 75 mm), مع ثلاث قيم من سرعة الدرفيل (0.5, 1, 1.5 m/s). و خمسة قيم من التخفيض بالسمك تم اختيارها لتغطية كل التساؤلات في هذا البحث.

بينت هذه الدراسة أن الزيادة في نصف قطر الدرفيل ستؤدي بالضرورة الى زيادة سمك طبقة سائل التزييت و عند نسب التخفيض العالية جدا فإن سمك طبقة سائل التزييت يصبح صغير جداً وهذا يستلزم استخدام سائل تزييت ذا لزوجة عالية.

</div>

1.   Introduction

In cold rolling process, the role of lubricant is to reduce the friction coefficient, guarantee the surface quality of products, and increase the tool life.Zhrgang et al[1] have carried out a series of experiments by using a rolling type tribometer to investigate the lubricity of the volatile lubricants at high speed forming. Experimental results show that the friction coefficient decreases with increasing working velocity for both SPCE and A3004, in any lubricant. With an increase of reduction in thickness the friction coefficient decreases for SPCEbt and increases for A3004.

Saxena[2]showed that the film thickness increases with an increase in R/h (roll radius to the strip thickness at the inlet ratio) .Zhrgang et al.[3] illustrates that with increasing rolling velocity, for a smooth work piece, the rubbed portions became slight, the slip bands became more marked and the friction coefficient decreases .The experiments of Kevin and John[4], showed that the viscosity of the oil in the emulsion did not have a major effect on the load .Increasing speeds cause a reduction of the loads at higher roll roughness but with the smoother rolls no speed effect was observed . Huart et al.[5] have done experiments to optimize the contact condition in cold rolling, the simulation of trapping shows the role of lubricant in cold rolling .The lubricant fills the cavity, and avoids a total flattening of the asperities .

K. Loaisil et al.[6] designed a new heating system to simulate interface temperature which has a decisive effect on lubricant behavior. These optimizations permit to analyze contact

temperature, forward slip and lubricant influence on friction, iron fine pollution and surface aspects. A great influence of temperature and lubricant on friction and wear has been put forward. An increase of the coulomb friction coefficient associated with a decrease of the iron fines quantity have been shown with an increase of temperature.

In this paper, the effect of some parameters like reduction in thickness, length of contact, rolling radius, viscosity of lubricant oil, and roll speed on the lubricant film thickness have been investigated. Computing of lubricant film thickness, roll separating force, length of contact and slide/roll ratio as a function of the process parameters are used to satisfy the objective.

2. Cold rolling process

Cold rolling is a metalworking process in which the metal is deformed by passing it through rollers at a temperature below its recrystallization temperature .Cold rolling increases the yield strength and hardness of a metal by introducing defects into the metal's crystal structure.
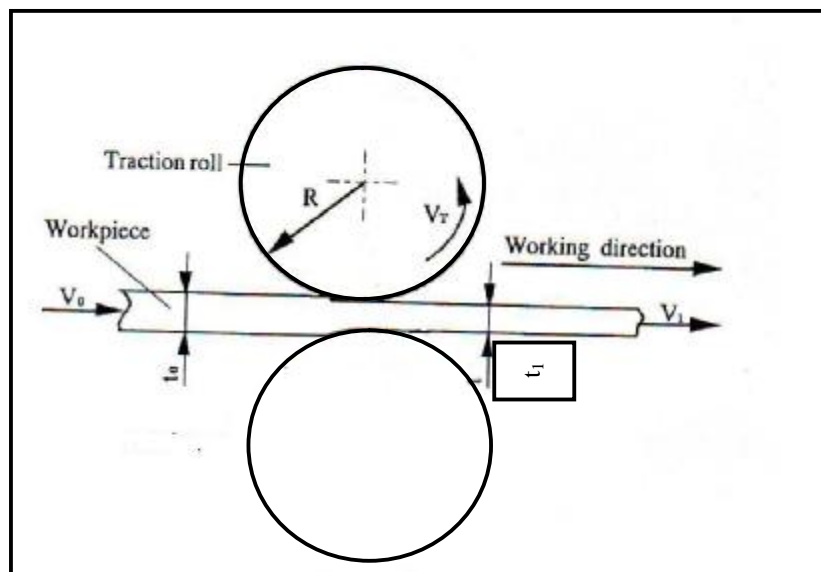

Figure (1) . A schematic diagram of the rolling process.

The gap between the rotating rolls is less than the thickness of the entering strip t_0 , therefore a friction force is necessary in order to bite the strip and to pull it through the rolls.A metal strip

passing through the rotating rolls is squeezed, and it elongates while its cross section area decreases .

The amount of deformation **"r"** achieved in a flat rolling operation (thickness reduction)is determined by the relationship [3]:

$$r =(t_o - t_1)/t_o \tag{1}$$

A machine used for rolling metal is called (Rolling Mill) .A typical rolling mill consists of a pair of rolls driven by an electric motor transmitting a torque through a gear .A force applied to the rolls in vertical direction is called (Roll Separating Force).

3. Material and lubricants

The strips are of stainless steel 304 .The strips are nominally 1 m long, 10 mm wide and 0.8 mm thick .Three oils are used A, B and C, the properties of the lubricants are given in Table (1) .

Table (1). Properties of the lubricants .

Lubricants	Viscosity (Pa.s)	Pressure-Viscosity coefficient (1/Gpa)
A	0.00507	11.28
B	0.0173	13.9
C	0.02186	14.58

The program conditions are given in Table (2).

Table (2).Program conditions.

Reduction in thickness(r%)	75, 80, 85, 90, 95
Rolling velocity V_T(m/s)	0.5, 1, 1.5
Slide/roll ratio δ	0.4, 1.42, 1.85
Traction roll radius (mm)	55, 65, 75

The lubricant film thickness, length of contact, angle of entry and the roll separating force are reported.

4. Results and discussion

Figure (2) shows the variation in the lubricant film thickness with increasing reduction in thickness, the lubricant film thickness decreases for any lubricant .The result in this figure compared with the results of Mizuno form[3] and a good agreement was found.
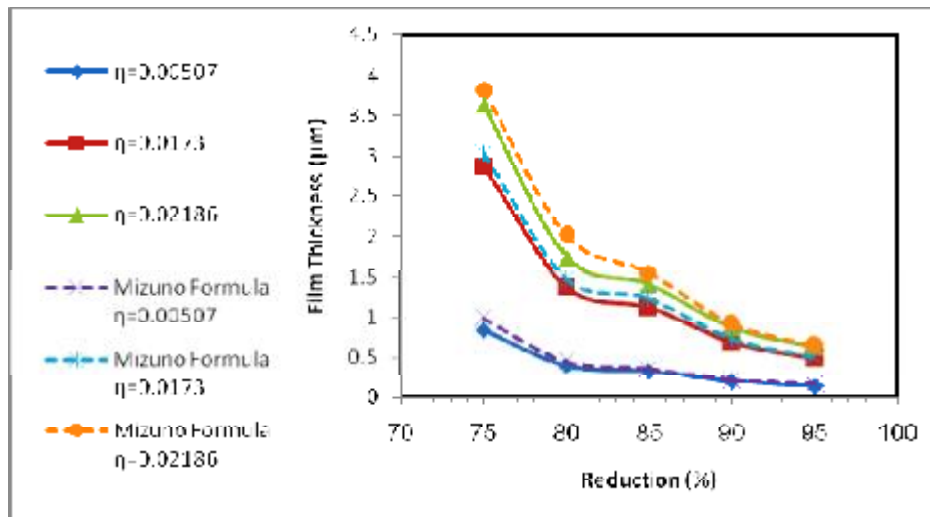
The effects of the length of contact on the lubricant film thickness are shown in Figure (3) .It is quite apparent that increasing length of contact increases the lubricant film thickness .The results of the dependence of the roll separating forces on the reduction are given in Figure (4) . The results indicate that, as expected, the roll separating forces increase with increasing reduction.

The magnitude of the lubricant film thickness is shown in Figure (5)as a function of slide/roll ratio (δ), with an increase of slide/roll ratio, the film thickness increases for any lubricant .Figure (6) shows the variation in the lubricant film thickness with rolling radius, the lubricant film thickness will increase with increasing rolling radius.
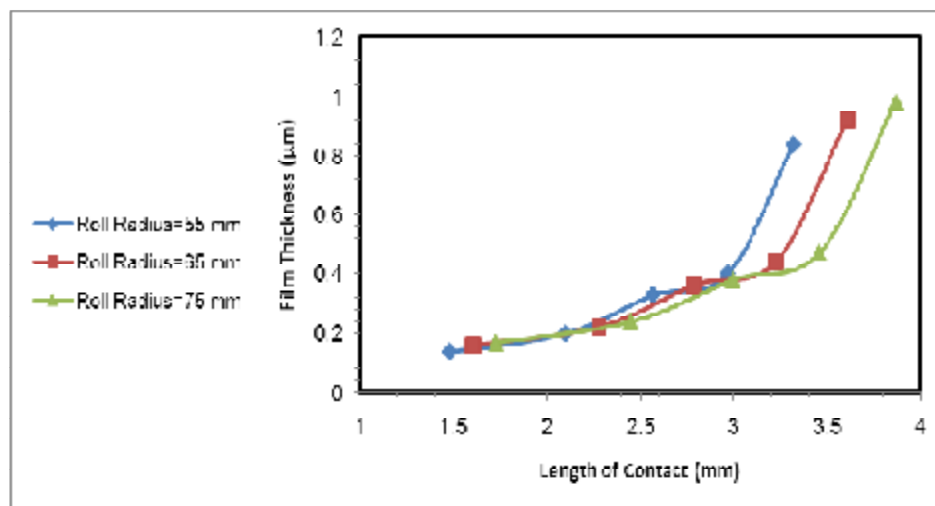
The increase in rolling velocity and hence, the relative velocity between the roll and the strip, is expected to entrain more of the lubricant, leading to lower frictional resistance, lower load on the mill and high lubricant film thickness .This is observed in Figure (7).

5. Conclusions

1) The film thickness decreases with increase in reduction, but increases with length of contact and rolling radius.
2) The roll separating force increases with increases in reduction.
3) With an increase in rolling velocity, the lubricant film thickness increases.

Figure (2). Variation of film thickness with reduction,

R=55 mm, V$_T$=0.5 m/s.

Figure (3).Variation of film thickness with length of contact ,
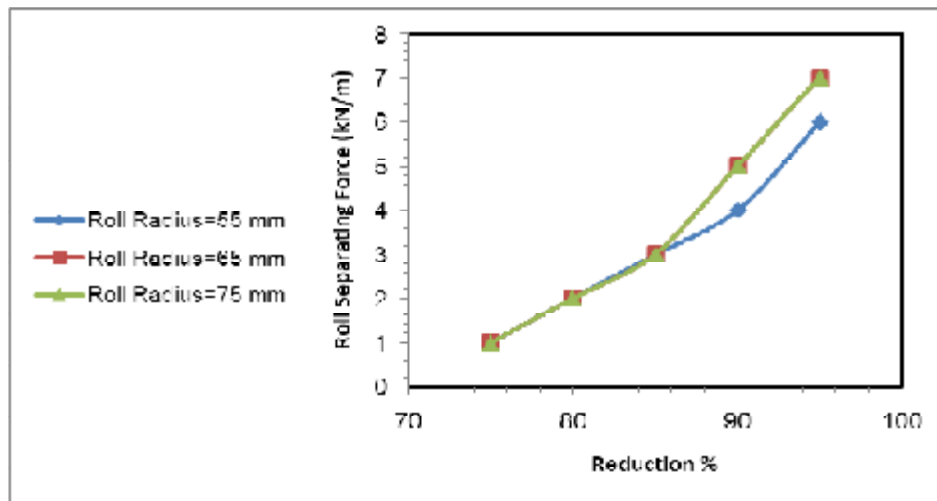
V$_T$=0.5 m/s , η=0.00507 Pa.s .

Figure (4). Variation of rolling separating force (kN/m) with reduction ,
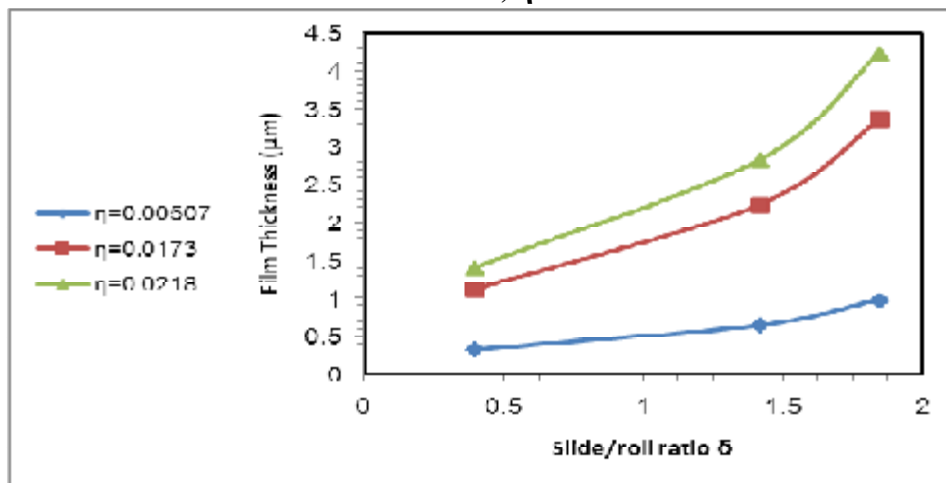**V_T=0.5 m/s , η=0.00507 Pa.s .**

Figure (5).Variation of film thickness with slide/roll ratio,
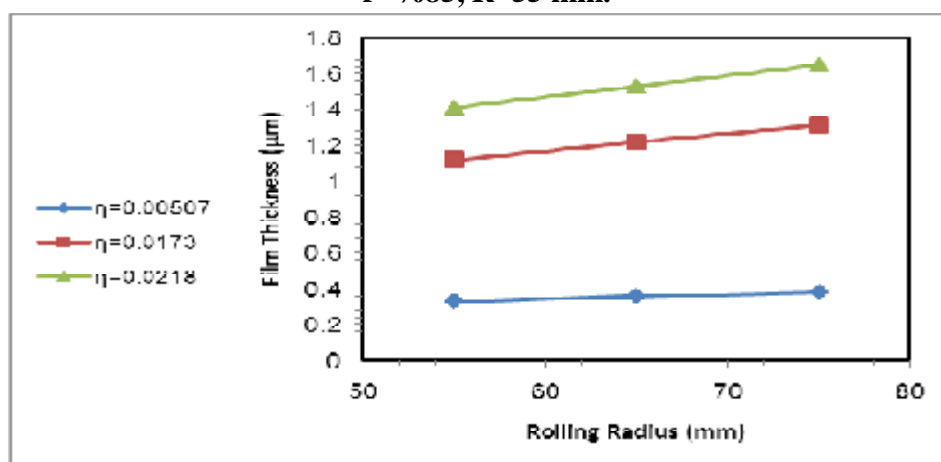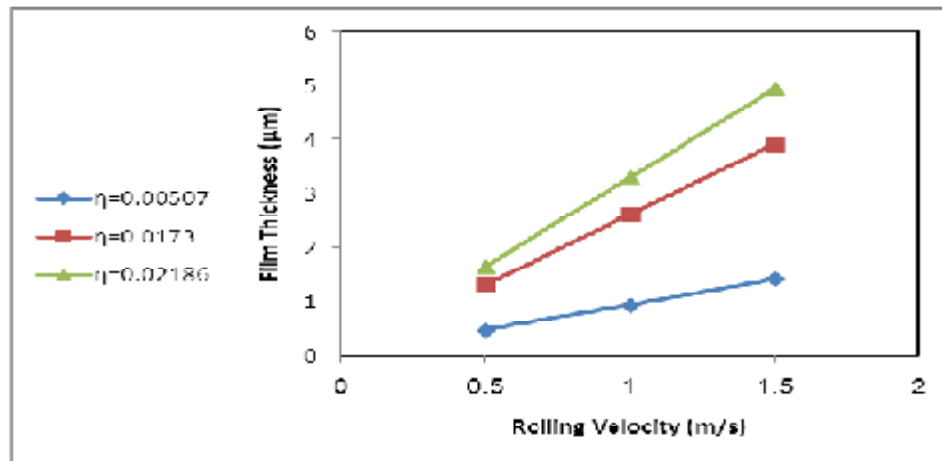**r=%85, R=55 mm.**

Figure (6) .Variation of film thickness with rolling radius (mm),
r=%85, V_T=0.5 m/s.

Figure (7). Variation of film thickness with rolling velocity (m/s),

r=%80, R=75 mm.

6. References

[1] Wang, Z., Dohda ,K. ,and Jeong, Y.H., 2003, "Lubricity of Volatile Lubricants in Sheet Metal Rolling", Journal of Materials Processing Technology, Vol. 140, pp. 548-554.

[2] Saxena, S., Dixit, P.M.,and Lal, G.K., 1996, "Analysis of Cold Strip Rolling Under Hydrodynamic Lubrication ", Journal of Materials Processing Technology, Vol. 58,pp. 256-266.

[3] Wang, Z., Dohda, K.,and Haruyama, Y., 2006, "Effect of Entraining Velocity of Lubricant and Sliding Velocity on Friction Behavior in Stainless Steel Sheet Rolling", Wear, Vol. 260, pp. 249-257.

[4] Dick ,K., and John, G., 2005, "The Effect of Roll Roughness and Lubricant Viscosity on the Loads on the Mill During Cold Rolling of Steel Strip",Journal of Materials Processing Technology, 168,pp. 16-24.

[5] Huart, S.,Dubar, M. ,Deltombe, R.,Dubois, A.,and Dubar, L., 2004, "Asperity Deformation, Lubricant Trapping and Iron Fines Formation Mechanism in Cold Rolling Processes", Wear, Vol. 257, pp. 471-480.

[6] Louaisil, K., Dubar, M., Deltombe, R., Dubois, A.,and Dubar, L., 2009, "Analysis of Interface Temperature, Forward Slip and Lubricant Influence on Friction and Wear in Cold Rolling", Wear, Vol. 266, pp. 119-128.

[7] Lenard, J.G., 2004, " The Effect of Roll Roughness on the Rolling Parameters During Cold Rolling of an Aluminum Alloy", Journal of Materials Processing Technology, Vol. 152, pp. 144-153.

[8] McConnell, C., and Lenard, J.G., 2000, "Friction in Cold Rolling of a Low Carbon Steel with Lubricants", Journal of Materials Processing Technology, Vol. 99, pp. 86-93.

[9] Lenard, J.G., 1998, "The Effect of Lubricant Additives on the Coefficient of Friction in Cold Rolling", Journal of Materials Processing Technology, Vol. 80-81,pp. 232-238.

7. Nomenclature

r   reduction in strip film thickness

R   roll radius

t_o strip thickness at inlet

t_1 strip thickness at outlet

V_o strip velocity at inlet

V_1 strip velocity at outlet

V_T roll velocity

Greek letters

δ   slide/roll ratio

η   viscosity of lubricant

Catalyzed Mechanism for Microwave Absorption in Composite Barriers

Ahmed K. Abed

**Electrical and Electronic Dept.
College of Engineering
Thi-Qar University**

S. S. Abdul Noor

**Applied Science Department
University of Technology**

A. M. Jasim

**Research and Development Department
Ministry of Sciences and Technology**

Abstract

A series of two-layered composite barriers filled with   (10% carbon black) were produced, with their second layers loaded with foreign dispersion acting in aid of the microwave absorption process. Fixed weights of chopped copper wires with lengths (1,3,5) mm were dispersed in the above mentioned barriers. The resulting behavior indicates that these catalyst dispersion played a very useful role in enhancing the absorption of the barrier. Moreover, certain wire lengths exhibited an optimum behavior at various frequencies, suggesting that these wires act as short dipole antennas which convert the microwave signal into a leaked current. Mixing various wire lengths yielded a (100% bandwidth covering the whole of the X-band fore reflectivity level less than −11dB). Also various concentrations of AL-powders were dispersed in these second layers and an optimum concentration exhibited a low reflectivity level over the whole X-band. Intermixing of wires and powders produced a rather poor behavior suggesting that this might be due to the metallic over exceeded presence in the barrier.

المستخلص

حُضيرت حواجز متراكبة من طبقتين محشوة بتركيز(١٠%) من مسحوق الكاربون الأسود.حيث إن الطبقة الثانية طعمت بمواد إضافية مشتتة لعبت دوراً محفزاً في عملية امتصاص الموجات الدقيقة.كذلك تم تطعيم الطبقة الثانية من الحاجز المتراكب بأوزان ثابتة من الأسلاك النحاسية المقطعة بأطوال مختلفة(١,٣,٥)مليمتر.التصرف الناتج أظهر إن المشتتات المحفزة لعبت دوراً مفيداً جداً في تعزيز امتصاص الحاجز للموجات الدقيقة.من ناحية أخرى, أطوال السلك في الحاجز المتراكب اظهرت تصرفاً مثالياً عند ترددات مختلفة من الحزمة مما يوحي بأن الأسلاك عملت كهوائي ثنائي قصير يقوم بتحويل إشارة الموجات الدقيقة إلى تيار متسرب داخل الوسط.تم الحصول على انعكاسية اقل من ١١- ديسيبل عند خلط أطوال مختلفة من السلك النحاسي وبعرض نطاق ترددي واسع ضمن الحزمة.أضيفت تراكيز مختلفة من مساحيق الألمنيوم للطبقة الثانية من

الحاجز المتراكب, عند تركيز معين لمسحوق الألمنيوم اظهرت انعكاسية قليلة على كل الحزمة الترددية. الخلط لمادة مسحوق الألمنيوم وأسلاك النحاس أبدى انعكاسية عالية بسبب زيادة نسبة المعدن في الحاجز.

1. Introduction

Radar wave absorbing barriers have become a center of attraction for many research groups, since the declaration of the stealth aircraft [1]. Prior to that the application has been mainly concerned with echoless chambers and few other applications[2]. The main factor affecting the detection capability of a certain airborne target is it's Radar Cross Section (*RCS*) at that frequency band. This is decided heavily by the geometry of the target, specially the overall size and the details of the shape. The (RCS) of target may be reduced by coating the target with Radar Absorbing Material (RAM)[3] .   A number of materials have been investigated and more may be still under investigation .The menu included the carbon black family [4], the family of ferrite and other chemicals [5]. These have been used in the form of simple (one-layer) barrier, a complex combination of layers [6,7] either of the same type but with different concentrations or different materials. The point of major importance is the nature of the material like its absorbance, it's dielectric constant, permeability, ε and μ respectively. Moreover, there are some criteria to be considered when a barrier is being developed, which are the reflectivity minimal and the bandwidth of the reflectivity. Their have been some work on complex barriers which suggested that the multilayer barrier should have a minimum value of   ε or μ at the inter layer boundary in order to make sure that the incoming microwave penetrates the barrier system. This would enhance the probabilities of absorbance loss of the microwave. This in fact has lead to the idea of using some foreign bodies imbedded within the absorbing medium, in order to stop the penetrated wave from leaving the barrier very quickly, or to transform the wave signal into some other form of power which may be deposited with the boundaries of the barrier.

The efforts of researchers were concentrated on two goals. The first goal, is reducing the reflectivity to the optimum level. The second, is reducing the thickness of the barrier and arriving at the painting technique. Unfortunately, these efforts were often unpublished and were top secret because they are used in military applications such as the stealth technology in fighter aircrafts.

However, we can mention some of these efforts .A multilayer barrier made of four layers of composted ferrites was investigated experimentally [5]. This completed absorber has a

performance of about -7 to -16 dB reflection loss over (8 to 18 GHz).The computed and measured reflection loss curves differ by about ±2dB in a way. The total thickness of four layers was 20 mm. A method of reducing the thickness of a ferrite absorbing wall and controlling the matching frequency characteristics by applying DC magnetic field, H_{dc} , perpendicularly to microwave magnetic field [8].By combining rubber with carbon and ferrite, a material having dielectric and magnetic losses is obtained[9].This material shows good absorbing characteristics when used in a single-layer structure backed with a conductor. The best absorber characteristics among the investigated combinations were obtained when the ratio of ferrite was equal to the ratio of carbon black in the hybrid single layer. In the C-band, its relative bandwidth in a single layer structure is up to 4.5 times wider than of nonmagnetic lossy dielectric material of the same thickness. Moreover, a multi-layer barrier made of six layers combined from simple layer (ferrite-epoxy) and hybrid layer (carbon and ferrite epoxy) was investigated experimentally [10],the total thickness of multi-layer structure was 3mm. The absorption performance is considered to be good results in 6.5 to 7.5 GHz for reflectivity level less than (-10 dB).From the results obtained that absorption increases when the thickness of layer increases.

It is aimed by this work to develop a new type of barrier not only of complex nature but also of hybridized layers. By doping these layers with absorption aids (or *catalysts*) like wires or metal powders in order to modify the mechanism of absorption or looseness of the material.

2. Experimental techniques

The basic matrix of the barrier consists of solid Novolak, which is powdered in the fine particulates, mixed with the proper catalyst and heated to *100C^o* until the mixture shows signs of fusion. The mixture is then crushed and mixed with appropriate amount of (*10 % carbon black*) and *catalysts (*Aluminum powder, wires Copper) fillers. The homogenized mixture is then hot pressed (10 ton) at 150 C^o for 30 minutes. The resulting disk-shaped specimen is then machined into rectangular cross section, with dimensions to suit the inner tube of the wave-guide[11].Two types of barriers were developed those of layer (simple), and those which consisted of multilayers each consists of different filler concentration.

The network analyzer as shown Figure(1) is characterized by high accuracy, high speed measurements, in addition to the scanning capability of the frequency band of interest, which

included the X-band. A (HP8510B) computer is interfaced with the above analyzer, and prior to any use the whole system is usually calibrated. Two measurement assembles were used, a two port and a single port arrangement as shown in Figure(2) and Figure(3) respectively .In case of the one port arrangement, both the transmitter and receiver are located on one end of the waveguide tube. The other end facing a metal sheet which is considered to be short circuit, because it is a perfect reflector. Normally, the specimens under investigation placed in between the short circuit plate and tightly filled under inside the waveguide opening.

This arrangement in fact is considered the nearest to the real situation. Moreover the scattering of microwaves at the edge of the inner tube of waveguide and specimen is expected to enhanced the reflectivity readings of the barrier. This of course is not applicable in actual practical situations ,which makes the waveguide results to be considered as modest in this scheme of analysis. The following formula of wave conservation is valid:

$$R^2+A^2=1 \tag{1}$$

Where

R=reflection coefficient.

A=Absorption coefficient.

In the second scheme of analysis (two-port arrangement) the waveguide tube openings are individually blocked by transmitter on one side and a receiver on the other side. In this scheme of analysis the following formula is valid

$$R^2+A^2+T^2=1 \tag{2}$$

Where

T=Transmission coefficient

The advantage of this arrangement is that it analyses the fine details of the interaction where the above three components of the interacted wave are immediately determined(R and T are measured ,A is calculated from (2)).

3. Results and discussion

A two-port arrangement was used to investigate the details of the microwave interaction with composite barriers between resin matrix filled with various concentrations (0-50%) of carbon black. From figure (4),it can be seen that the carbon black filler seems to offer an optimum effect at (10%) presence, where the overall reflectivity is minimum and the absorption is found to be

maximum. In order to design and control the absorption process it might be interesting to use some looseness-aid or catalysts to enhance the absorption .These added inclusions are thought to force the penetrated microwave to travel in a new region before leaving the barrier, so that   a complex barrier was arranged in such a way as shown in the Figure (5). A first layer (3mm thick) containing (10%) carbon black is followed by a second layer of the same nature and thickness, but further composited by dispersing small amount of chopped copper wires (50μm diameter). The length of these wires was chosen to be (1,3,5mm) each was dispersed in separate barriers. Each complex barrier contains in its second layer a total weight of (0.5gm) of copper wires, which forms about (10 wt.%) of the second layer. The results of measurements made on these complex wire-dispersed barriers are shown in Figure (6). The behavior exhibited in this figure suggests that the presence of the dispersed wires have modified the behavior of a (6mm thick.) composite barrier containing (10%) carbon black filler only. Moreover, the modification reflected upon the bandwidth of the reflectivity level in a way that attracts attention. Moreover, it may also be noticed that the overall reflectivity loss seems to be affected by a certain correlation, between the length of the wire and the frequency of the penetrating wave. This may be further clarified by the values listed in Table (1) below.

Table(1).Relationship between catalyst wire length and wavelength.

Freq. GHz	Reflectivity level dB			Length of wire / λg		
	1mm wire	3mm wire	5mm wire	1mm /1g wire	3mm /1g wire	5mm /1g wire
8	-5.5	-8	-11	1 /67.4	1 /22.4	1 /13.4
9	-9	-7	-9	1 /49.4	1 /16.4	1 /10
10	-11	-10.5	-3	1 /40	1 /13.3	1 /8
11	-16	-9.75	-3.5	1 /34.2	1 /11.3	1 /6.8
12	-12.5	-10	-4	1 /30	1/10	1 /6

Here, it is obvious that the overall reflectivity level depends explicitly on the length of the dispersed wires. The (5mm) wire seems to enhance the absorption of the composite barriers at the lower end of the frequency range.

On the other hand, the (3mm) and the (1mm) dispersed wire seem to enhance the absorption at the higher frequency range of the X-band. This in fact raise a question about the relation between the wire length and the wavelength of the penetrated microwave. This may in fact be clarified by the deduced correlation between the length of the wire and λg (wavelength inside the waveguide), also listed in the Table (1).

It was noted that a maximum absorption is exhibited when the ratio of (wire length / λg) is about (1 /13.4).When this is converted into the case of free space the ratio of (wire length / λo(wavelength in free space)) is found to be very near to (1/10) which represents the case of *short* dipole antenna[12]. On the other hand, the (1mm) wire lengths did not conform to this hypothesis, since the above mentioned ratio was deduced to be in the region of (1/34-1/40). However, this may be correlated with triple the wavelength of (21GHz) frequency, where it represents the resonance frequency of the short dipole antenna of (1mm) long wire. Hence, the overall behavior of the (1mm) wire may also be explained in terms of the short dipole antenna.

By looking back on Table(1) it is noticeable that the maximum value for absorption in the (1mm) wire dispersion is higher than those in the case of (3mm) and (5mm)-wire dispersion. This may be discussed in terms of the electric currents that may be conducted and leaked by the medium. Since the microwave signals received by the wires are converted into electric currents to be leaked into the medium. The number of the (1mm)-wire pieces present in the hybrid is higher than that in the case of (3mm) and (5mm) wire dispersions. Hence, this layer presence of wire pieces would represent an enhanced conduction capability. Moreover, shorter wires would pose lower total resistance to the passing current, which should result into the passage of higher currents. Therefore, the overall behavior of the hybrid layer would suggest that shorter wires would help the absorption mechanism more than longer wires. This may be reflected as an enhanced imaginary part of the dielectric constant[13].

The above discussion may lead to the fact that the first layer of this complex barrier is making a good or rather transparent to electromagnetic waves. Whereas, the second layer is acting as a resonator to this complex system[14].

From the above discussion it was interesting to investigate the effect of mixed lengths in the hybrid layer, which was realized by a complex barrier whose second layer contains a mixture of (1mm) and (5mm) wires in a total presence of (0.5 gm). Also a second method of mixing was realized where the wire's lengths ranged between (1-5mm), and in a total presence of (0.5 gm).

Test results shown in Figure (7) indicate the effectiveness of this further hybridization, where the bandwidth in both cases was enhanced to cover 100% of the X-band fore reflectivity level less than (-11dB). However, the reflectivity values were lower in the case of a mixture of (1mm) and (5mm) only.

In a general comparison of all the above complex and hybridized barriers it might be worthwhile to consider the behavior of a (6mm) simple barrier containing (10% carbon black). The difference in the behavior may be considered as qualitative, and the complex / hybrid barrier may be considered as a different class of material all to gather.

Another type of hybridization to the second layer was made by dispersing various quantities (0.05gm-0.3gm) of aluminum powders. The aim was to investigate the effect of the fineness of the particles on the general absorption of the barrier.

Table(2).Frequency response of catalyzed complex barrier filled with AL-powder.

Freq. GHz	Reflectivity Level dB			
	0.05gmAl	0.1gmAl	0.2gmAl	0.3gmAl
8	-8	-11.7	-8.5	-8
9	-7.5	-11.5	-10	-9
10	-8	-11	-8	-4
11	-8	-11	-8	-3.5
12	-8.25	-11.2	-6	-3

The results are shown in Figure (8). and the measured values are listed in the Table (2). above. The barrier containing (0.1gm AL) exhibited an optimum reflectivity value at 10 GHz Fig(7). Beyond that, higher powder dispersion seemed to enhance the reflectivity level in an undesirable manner.   The bandwidth of the optimum concentration was (100% over the X-band), with a reflectivity level less than (-11dB).The expected mechanism that governed the behavior of

the powder dispersed barrier is thought to be that the aluminum particles act as scattering centers homogeneously dispersed throughout the second layer. These centers would act in a manner, which prolong the paths traveled by the penetrated microwave, thus enhancing the chance of these waves to be absorbed by the lossy medium. Hence, the powder is acting as a catalyst, which prolongs the time and length of flight of microwave within the barrier. It was thought to be quite interesting to mix both additive dispersion (wires and Al powders) in a single hybrid, and to study the behavior of this new type of hybrid. A new set of complex / hybrid barriers were produced and their mixed dispersion were fixed as listed in Table (3) . The general overall behavior was not up to the standard set by the wire-dispersed or the powder-dispersed barriers. However , the mixed dispersion containing (5mm wires and 0.1gm Al) gave modestly better results. This observed draw back might be due to the exceeded overall presence of metallic scattering centers, which could have affected the nature of the complex barrier negatively.

Table (3) .Frequency response of catalyst complex barriers doped with Cu-wire and AL-powder.

Freq. GHz	*Reflectivity Level dB*			
	1 mm wire + 0.1 gm AL	5 mm wire + 0.1 gm AL	1,5 mm wire + 0.1 gm AL	1-5 mm wire + 0.1 gm AL
8	-6	-7	-6	-7
9	-7	-10	-7	-6.5
10	-7.5	-11	-6.5	-6
11	-8	-7	-7.5	-5
12	-7	-7	-7.5	-7

4. Conclusions

Composite material filled with 10% carbon black has shown good behaviors to microwaves absorption. The principal of complexing the barriers resulted in an explicit broading of the frequency band and in enhancing the absorption in non linear manner. The wire catalysts acted as antennas, which received microwaves and then leak it to the lossy medium . The catalyst metal

particles acted as scattering centers which prolonged the path of the microwave within the hybrid barrier. The catalysts metal-wires may also act mechanically to reinforce the composite matrix.

5. References

[1] Adam, J., April 1988, "How to Design an Invisible Aircraft", pp.26-31, IEEE Spectrum.

[2] Freeman , R. , 1982,"Interference Suppression Techniques for Microwave   Antenna & Transmitters", Artech   House Inc. .

[3] Willaims ,N., February 1987, "Radar Cross Section (RCS):Engineering for Stealth", Electronic Engineering .

[4] Kwon ,S. K., Ahn ,J.M. , Kim ,G. H. and Chun, C. W., 2000,"Microwave Absorbing Properties of Carbon black/Silicon Rubber Blend in the GHz Range" , Proc. of the 3th Conference on National Defence materials,pp.c161-c169, ,.

[5] Amin, M. B. and James, J.R., May 1981,"Techniques for Utilization of Hexagonal ferrites in Radar absorbers. Part1: Broadband Planar Coatings", Radio Electron. Eng. (London), vol.51, pp. 209-218.

[6] Folgueras, L. C., Alves ,M. A., Martin, I. M., and Rezende ,M. C., march 2009,"Single- and Multilayer Microwave Absorbing Material Based on Conducting Polyaniline and Polyurethane Polymers for operation in the X-band",Progress In Electromagnetics research Symposium,Beijing,china,pp.23-27.

[7] Parida , R. C. , Singh, D. & Agarwal, N. K., April 2007, "Implementation of Multilayer Ferrite radar absorbing coating with genetic algorithm for Radar Cross Section reduction at X-band",Indian Journal of Radio& Space Physics,Vol.36,pp.145-152.

[8] Kotsuka ,Y., Sept.1989,"Characteristics of a Broadband and Thin Ferrite Absorbing Wall", IEEE Trans. On EMC , Vol .2, pp.(780-783).

[9] Mirtaheri ,S. A., Yin, J., Seki, H., and Natio, Y., Sept.1989,"The Characteristics of Electromagnetic wave Absorbers Composed of Rubber,Carbon and Ferrite",IEEE Tras. on EMC,Vol.2,pp. (784-787).

[10] Iliev, Sept.,1994, "Multilayer Microwave Absorbers for 6.5-10.5 GHz Frequency Range",Proc.14th Int. Conf. Microwave Ferrites,Bulgaria,.

[11] HE , .B. , 1967, "Measurement of RF Properties of Materials, A survey", Proceedings of the IEEE,Vol.6,pp. (1053-1056).

[12] Roy Blake, 1993,"Basic Electronic communication",West publishing company.

[13] Xiucheng ,Z., Sep.,1994,"Temperature Character of Complex Permeability and Permittivity of Microwave Ferrite Absorbent",Proc.14th Int.Conf.Microwave Ferrites,Bulgaria.

[14] Elbakly, M., 2009," Design of Double - Layer Rubber Radar Absorbing Sheet" , OJEEE,Vol.1,No.1.

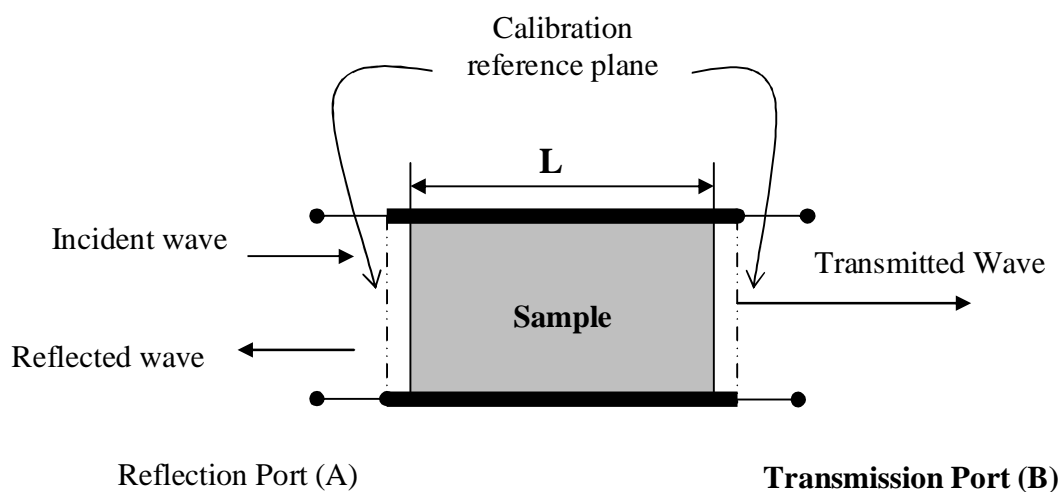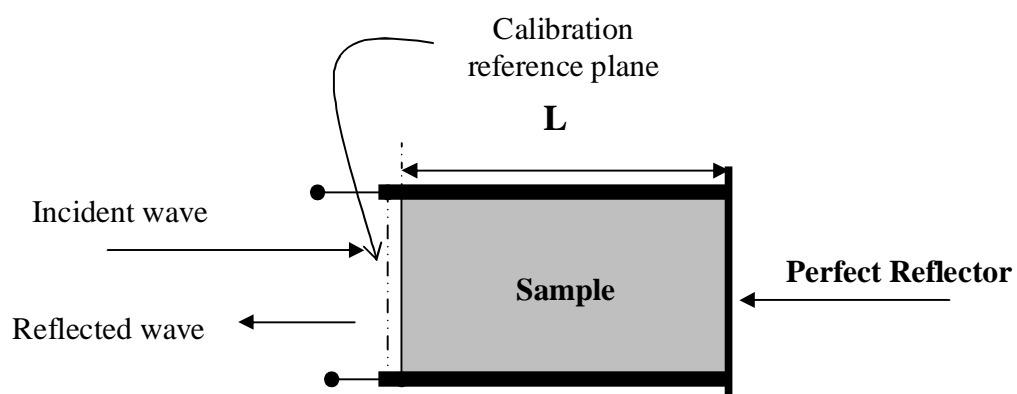**Figure (1). Network analyzer HP8510B.**

Calibration reference plane

L

Incident wave

Transmitted Wave

Sample

Reflected wave

Reflection Port (A)

Transmission Port (B)

Figure (2). Two ports measurement .

Calibration reference plane

L

Incident wave

Perfect Reflector

Sample

Reflected wave

Figure (3). One port measurement .

(A)

(B)

(C)

Figure (4). Frequency response for different weight percent of carbon black .

(A) Reflection coefficient ,(B) Transmission coefficient and (C) Absorption coefficient.

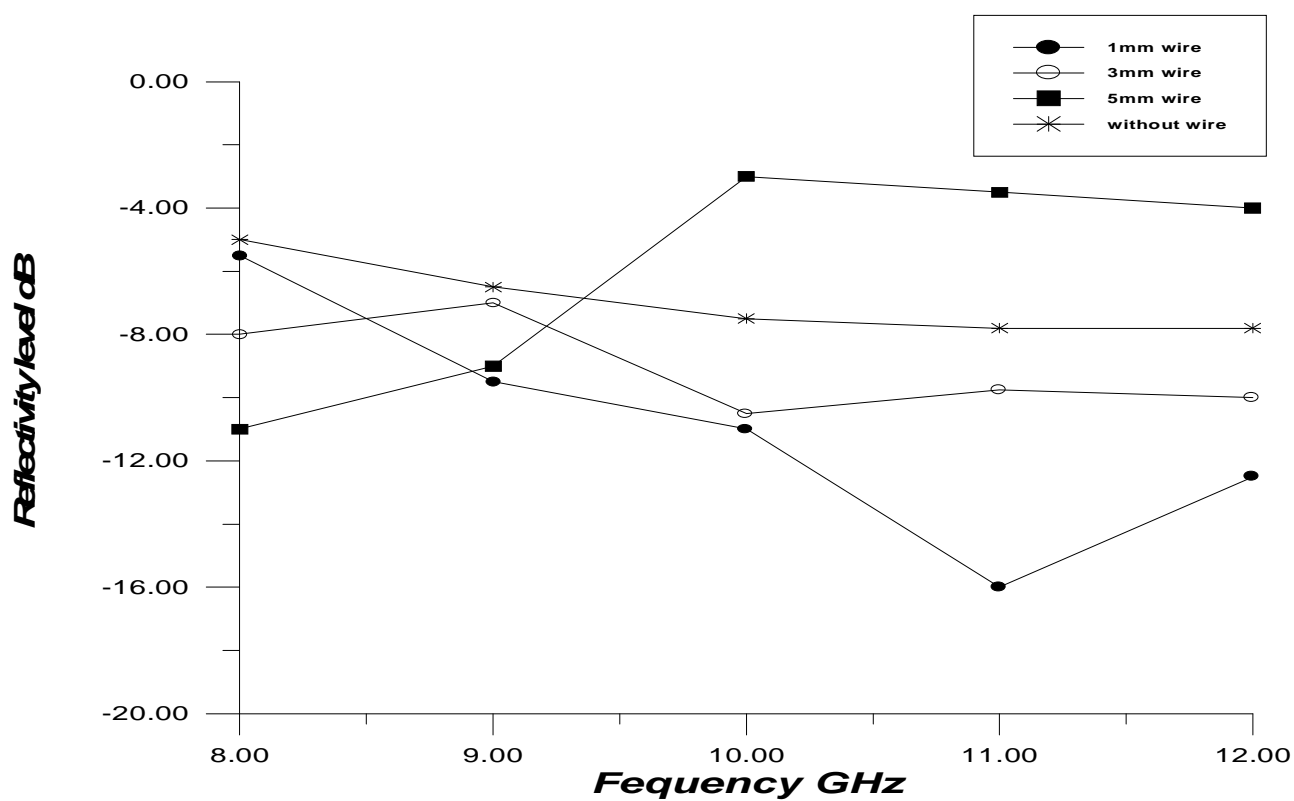**Figure (5). A catalyzed two-layer composite barrier .**

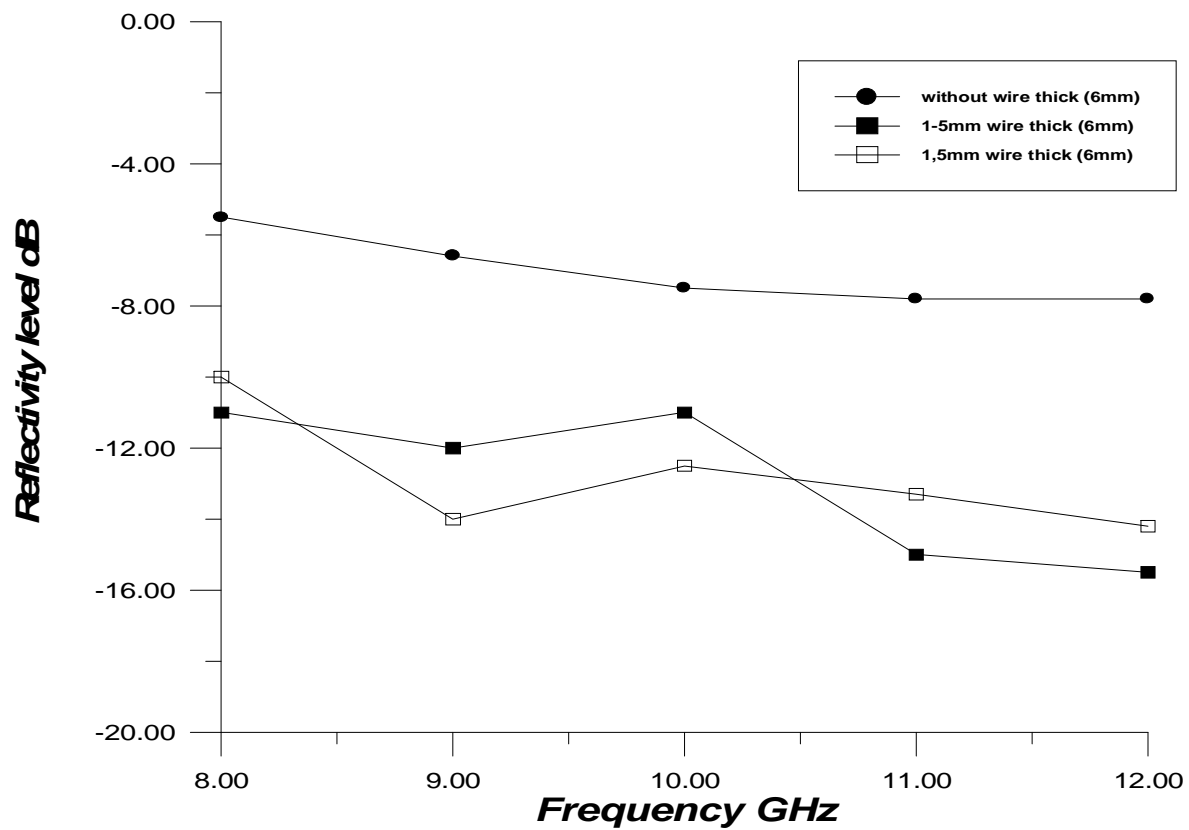**Figure (6). Relationship between wire length and frequency .**

Figure (7). Comparison between single barrier(10% C) and catalyst barriers .
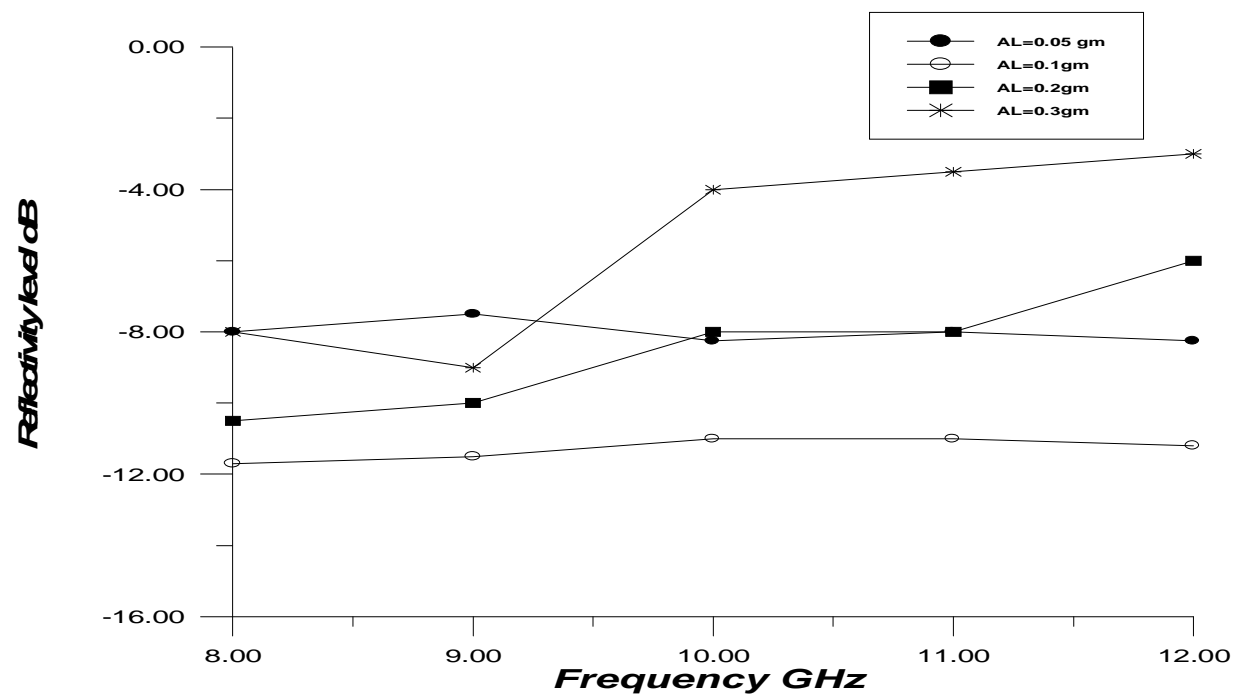

Figure (8). Reflectivity level of catalyst barrier versus frequency for different AL weight .

Numerical Investigation of Hydrodynamic Characteristics of the Micro Irrigation Lateral

Mushtaq Ismael Hasan

Mechanical Engineering Department
College of Engineering
Thi-Qar University

Abstract

In this paper , the analysis of the hydraulics of micro irrigation lateral is made and the effect of the design parameters (ground slope, length of lateral and velocity of flow) on the hydrodynamic performance of this lateral pipe is numerically studied. The numerical solution for this model is made using the finite difference method which considered accurate and simple compared with other analytical and numerical methods used in literature to study micro irrigation systems.

The numerical model used in this paper is validated by comparing its results with results of another numerical methods presented in literature .The results obtained show that, the parameters studied in this paper play an important role on the hydrodynamic performance of the micro irrigation systems.

<div dir="rtl">

التحليل العددي للخصائص الهيدروديناميكية لمنظومات الري بالتنقيط

المستخلص

في هذا البحث تمت دراسة وتحليل هيدروليكية منظومات الري بالتنقيط وتأثير بعض العوامل التصميمية (ميلان الأرضية، طول الأنبوب، سرعة الجريان) على كفاءة هذه المنظومات. تم حل النموذج الناتج من الاشتقاق باستخدام طريقة الفروقات المحددة والتي تعد من الطرائق العددية الدقيقة والسهلة مقارنة بالطرائق التحليلية والعددية الأخرى المستخدمة من قبل العديد من الباحثين في هذا المجال.

تم التحقق من دقة النموذج العددي المستخدم وذلك بمقارنة نتائج الحل العددي مع نتائج طرائق عددية اخرى مستخدمة من قبل احد الباحثين.من النتائج تبين لنا مدى التأثير الكبير والفعال لهذه العوامل على الاداء الهيدروديناميكي لهذه المنظومات وكذلك دقة وايجابيات طريقة الفروقات المحددة.

</div>

1. Introduction

Micro irrigation systems can deliver water and nutrients in precise amounts and at controlled frequencies directly to the application. With micro irrigation systems an extensive network of pipes is used to distribute water to emitters which discharge it in droplets, small streams or through mini-sprayers.

It is important to calculate the pressure distribution and emitter discharge correctly along the lateral. Using equations of energy and mass conservation give two partial differential equations system. These equations describe the flow in the lateral; their solution is tedious because of interdependence of the discharge and the pressure in a non linear relation. The solution of these equations cannot be completely analytic due to the empiric relation of discharge emitters and the energy loss relations. The numerical methods are often used to determine pressure and discharge in micro irrigation lateral.

There are many researchers in literature studied the micro irrigation units by different methods.

Wu and Gitlin (1975) [1] used the energy-gradient line (EGL) method to determine the lateral pressure head and flow rate profiles.

Anyoji and Wu (1987) [2] developed a statistical approach based upon the coefficients of variation of pressure head along a lateral line.

Warrick and Yitayew (1988) [3] used a nonlinear, second-order, ordinary differential equation (Differential method DM) in which the emitters are considered to be close enough for the lateral to be regarded as a homogeneous system of main tube and a longitudinal slot. In a later study Yitayew (1989) [4] presented a simplified analytical approach for the determination of total friction head losses which is an extension of the previous analytical solution.

Scaloppi and Allen (1993) [5] derived a differential approach to multiple outlet pipes with constant and continuously variable outflow.

Hathoot et al (1993) [6] used the forward-step calculation method which was applied to accurately establish the head loss caused by friction in any pipeline.

Kang and Nishiyama (1996) [7] used a finite-element scheme and polynomial lateral flow rate equation to determine pressure and outflow distributions.

Valiantzas (1998) [8] used the constant discharge method (CDM) and variable discharge method (VDM).

Vallesquino and Luque-Escamilla (2001) [9] presented an alternative approach based on the successive – approximations method (SAM) for solving lateral hydraulic problems for laminar or turbulent flow.

Valianzas (2002) [10] presented a new analytical approach for designing multi diameter irrigation laterals, in this method analytical equations were presented for the case of obtaining a general solution by direct calculation.

Lakhdar zella and Ahmed Kettab (2002) [11] used the Range Kutta and control volumes (CVM) numerical methods to analyse the hydraulics of the lateral micro irrigation.

Demir et al (2004) [12] developed model using dimensional analysis for frictional losses in drip irrigation laterals with cylindrical type in-line emitters placed at different spacing. They found that the mathematical model may be used to determine frictional losses in drip laterals.

 Zella et al (2006) [13] designed a micro-irrigation system based on control volume method using the back step procedure. The design consists of exploring an economical and efficient network to deliver uniformly the input flow rate for all emitters. This program permitted the design of large complex network of thousands of emitters very quickly.

In this paper the finite difference numerical method is used to analyse the hydraulics of micro irrigation lateral and the effect of some of design parameters on the hydrodynamic performance of this type of irrigation systems.

2. Mathematical model

To derive the mathematical model of the micro irrigation lateral the continuity equation must be applied and the principle of energy conservation on the elemental control volume on the lateral between two points i and i+l as shown in Figure (1).
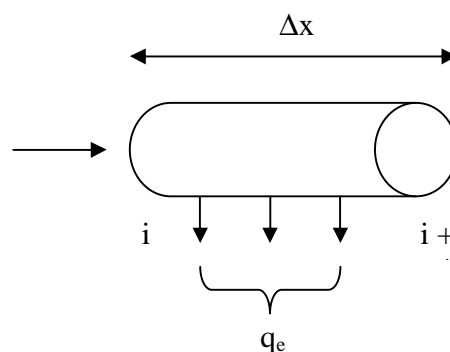

Figure (1). Control volume of micro irrigation lateral.

Continuity equation

$$AV_i = A\,V_{i+l} + q_e \tag{1}$$

Energy conservation equation

$$E_i = E_{i+l} + hf \tag{2}$$

Where:

V: flow velocity between i and i+l.

E_i and E_{i+l}: input and output energy head of water flow.

$q_{e:}$ individual emitter discharge given as the follows [14]:

$$q_e = C\,H^y \tag{3}$$

In which H is the pressure head in the lateral pipe at the inlet of emitter under consideration, C is the emitter coefficient and y is the emitter exponent which characterizes the flow regime and emitter type. Values of y should range from zero for a pressure – compensation emitter to 1 for an emitter in laminar flow regime.

Applying the energy conservation equation on the same elemental control volume to give the Bernoulli's equation:

$$H_i + \frac{1}{2g}V^2{}_i + Z_i = H_{i+l} + \frac{1}{2g}V^2{}_{i+l} + Z_{i+l} + hf \tag{4}$$

Where:

hf is the head loss between i and i+l along length (Δx) and its expression is given by the Hazen-Williams formulation represented by:

$$hf = a\,v^m\,\Delta x \tag{5}$$

There are three conditions of inclination along the lateral which are zero slope (horizontal), upward and downward slope.

Zero slope condition:

Where $Z_i = Z_{i+l} = 0$

Equation (4) becomes:

$$H_i + \frac{1}{2g}V^2{}_i = H_{i+l} + \frac{1}{2g}V^2{}_{i+l} + hf \tag{6}$$

After expansion of the terms H_{i+l} and V_{i+l} in equation (6) we obtain:

$$H_i + \frac{1}{2g}V^2_i = H_i + \frac{\partial H_i}{\partial x}dx + \frac{1}{2g}(V^2_i + 2V_i\frac{\partial V_i}{\partial x}dx + (\frac{\partial V_i}{\partial x}dx)^2) + hf \qquad (7)$$

Neglecting the term $(\frac{\partial V_i}{\partial x}dx)^2$ equation (7) becomes:

$$\frac{\partial H}{\partial x}dx + \frac{V}{g}\frac{\partial V}{\partial x}dx + hf = 0 \qquad (8)$$

Expansion the term V_{i+l} in equation (1) gives:

$$A\frac{\partial V}{\partial x}dx + q_e = 0 \qquad (9)$$

The flow regime is determined by Reynolds number.

$$\text{Re} = \frac{VD}{m} \qquad (10)$$

When Re > 2300, m = 1.852 and the value of a is given by the following equation when the Hazen - Williams formula is used [11].

$$a = \frac{K}{S^m A^{0.5835}} \qquad (11)$$

When Re < 2300, m = 1 and a is as following:

$$a = \frac{32m}{gD^2} \qquad (12)$$

Where S is the Hazen - Williams's coefficient, K is the coefficient, m is the exponent describing flow regime, g is the gravitational acceleration.

Combining equations (3), (5), (8), (9) and (12) give the following system of equations:
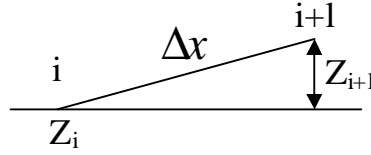
$$\frac{\partial V}{\partial x} = -\frac{C}{A\Delta x}H^y \qquad (13)$$

$$\frac{\partial H}{\partial x} = -aV^m + \frac{V}{g}\frac{C}{A\Delta x}H^y \qquad (14)$$

This system of equations represents the variation of pressure and velocity of flow in horizontal microirrigation lateral.

Upward slope condition:

Where $Z_{i+1} > 0$

Equation (4) becomes:

$$H_i + \frac{1}{2g}V^2{}_i = H_{i+l} + \frac{1}{2g}V^2{}_{i+l} + (Z_{i+l} - Z_i) + hf \qquad (15)$$

Let $Z_{i+l} - Z_i = \Delta Z$

$$H_i + \frac{1}{2g}V^2{}_i = H_{i+l} + \frac{1}{2g}V^2{}_{i+l} + \Delta Z + hf \qquad (16)$$

After expansion, substitution and arrangement of equation (16) give:

$$\frac{\partial H}{\partial x} = -aV^m + \frac{V}{g}\frac{C}{A\Delta x}H^y - \Delta Z \qquad (17)$$
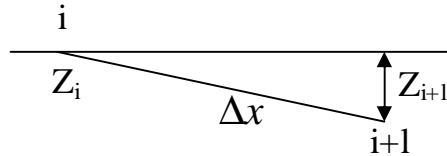
And the system of equations which represent the variation of pressure and velocity in upward slope micro irrigation lateral is:

$$\frac{\partial V}{\partial x} = -\frac{C}{A\Delta x}H^y \qquad (18)$$

$$\frac{\partial H}{\partial x} = -aV^m + \frac{V}{g}\frac{C}{A\Delta x}H^y - \Delta Z \qquad (19)$$

Downward slope condition:

Where $Z_{i+1} < 0$

Equation (4) becomes:

$$H_i + \frac{1}{2g}V^2{}_i - Z_i = H_{i+l} + \frac{1}{2g}V^2{}_{i+l} - Z_{i+1} + hf \qquad (20)$$

$$H_i + \frac{1}{2g}V^2{}_i = H_{i+l} + \frac{1}{2g}V^2{}_{i+l} - Z_{i+1} + Z_i + hf \qquad (21)$$

$$(22)$$

$$H_i + \frac{1}{2g}V^2_i = H_{i+l} + \frac{1}{2g}V^2_{i+l} - \Delta Z + hf \tag{22}$$

Note that the negative sign for Z_i in equation (20) is due to its respective elements and the value of Z_{i+l} will be Z_i for the next elements.

$$\frac{\partial H}{\partial x}dx + \frac{V}{g}\frac{\partial V}{\partial x}dx - \Delta Z + hf = 0 \tag{23}$$

After substituting the value of hf in equation (23) and arrangement, the system of equations in case of downward slope lateral becomes:

$$\frac{\partial V}{\partial x} = -\frac{C}{A\Delta x}H^y \tag{24}$$

$$\frac{\partial H}{\partial x} = -aV^m + \frac{V}{g}\frac{C}{A\Delta x}H^y + \Delta Z \tag{25}$$

The systems of equations (13), (14), (18), (19), (24) and (25) must be solved in suitable method.

Lakhdar Zella and Ahmed Kettab in ref. [11] solved simple horizontal lateral by using Range Kutta and control volumes methods. In this work the derived systems will be solved by using finite difference method and the effect of different parameters on the design of lateral will be studied.

3. Numerical solution

As mentioned before the finite difference method is used to solve the mathematical model derived in the previous section. One of the first steps to be taken in establishing a finite-difference procedure for solving a PDE is to replace the continuous problem domain by a finite-difference mesh as follows [15]: where the case of horizontal lateral is explained below as an example on the other studied cases.

The PDE system to be solved is:

$$\frac{\partial V}{\partial x} = -\frac{C}{A\Delta x}H^y$$

$$\frac{\partial H}{\partial x} = -aV^m + \frac{V}{g}\frac{C}{A\Delta x}H^y$$

The one dimensional forward difference representation is:

$$\frac{\partial u}{\partial x}\Big|i = \frac{u_{i+1} - u_i}{h} \tag{26}$$

Substitution of equation (26) in the above PDEs gives :

$$\frac{V_{i+1} - V_i}{\Delta x} = -\frac{C}{A\Delta x}(H_i)^y$$

$$V_{i+1} = V_i - \frac{C}{A}(H_i)^y \tag{27}$$

And $\dfrac{H_{i+1} - H_i}{\Delta x} = -a(V_i)^m + \dfrac{V_i}{g}\dfrac{C}{A\Delta x}(H_i)^y$

$$H_{i+1} = H_i - a\Delta x(V_i)^m + \frac{C}{gA}V_i(H_i)^y \tag{28}$$

4. Results and discussion

4.1. Verification

To check the validity of the present numerical model used in this paper, a verification is made by solving the model presented in [11] using the present model (finite difference method) and the results are compared with both methods used in [11] which are Range Kutta and control volumes methods.

A micro irrigation lateral model presented in [11] has the following specifications: total length is 250 m and internal diameter is 15.2 mm along this lateral 50 similar emitters were placed with equal interval. The characteristics of emitter used in empirical relation (3) are C = $9.14*10^{-7}$, exponent y = 0.5, s = 150, m = 1.852, K = 5.88 and g = 9.81 m/s^s. $\mu = 10^6$ m^2/s, initial pressure H_{max} = 30 m and initial velocity V_{max} = 1.2 m/s.

Substitution of these values in equations (27) and (28) in case of slope = 0 gives:

$V_{i+1} = V_i - 0.005\ (H_i)^{0.5}$

$H_{i+1} = H_i - 0.418\ (V_i)^{1.852} + 0.00051\ V_i\ (H_i)^{0.5}$

Figures 2 and 3 show the distributions of velocity and pressure along horizontal lateral as a comparison between finite difference method which is used in this paper and the methods of [11] (RK and CV methods). From these figures it can be seen that, there is a good agreement between

the results of these three methods. Also the curve represents FDM is located between two curves of RKM and CVM which shows the accuracy of the present model.
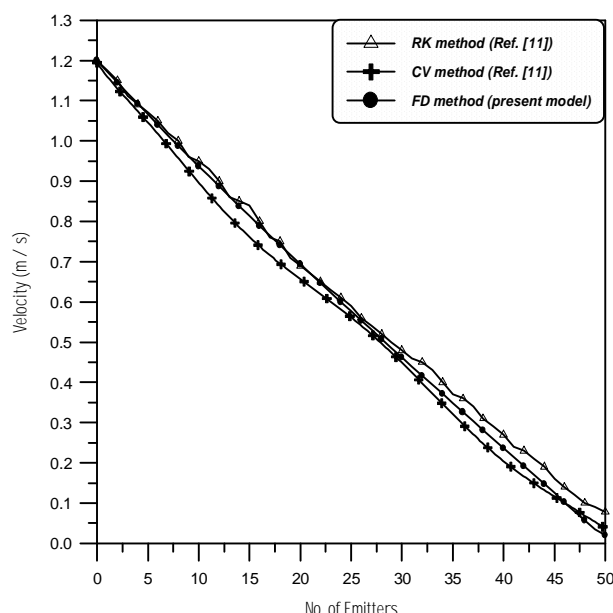

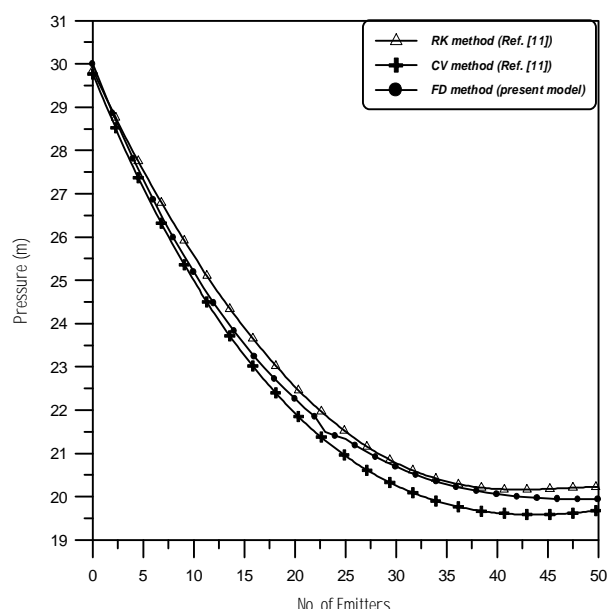**Figure (2). Velocity distribution along lateral as a comparison   between different methods.**

Figure (3). Pressure distribution along lateral as a comparison between different methods.

    After checking the accuracy of the present model computer programs developed to calculate the distribution of pressure and velocity at the emitters along the lateral with different slope conditions. Also to calculate the effects of other parameters such as length of lateral and initial velocity.

4.2. Effect of slope

    Figures 4 and 5 show the effects of lateral slope which have either a positive or negative effect on the distribution of the pressure and flow rate along lateral.

     Figure (4) shows the distribution of pressure in the successive emitters along lateral for different slope conditions (horizontal, downward and upward slope). From this Figure it can be seen that, the sloped up lateral always results an increase in pressure losses along the lateral length and these losses increased with increasing the slope due to the friction and gravity effects. And the downward slope reduces the losses.

Figure 5 shows the distribution of flow rate in the successive emitters along. The lateral for different slope conditions (horizontal, downward and upward slope). From this figure one can observe that, the lateral with downward slope can deliver flow rate more than that for horizontal lateral for the same emitter. While the flow rate decreased for upward slope and the reduction in flow rate increased with increasing the slope due to the friction and gravity effects.

From the previous results shown in Figures 4 and 5 it can be seen that, the ground slope has high effect on the design of lateral of micro irrigation system since the small change in Δz (difference between the elevations of two successive nodes) caused effective influence on both the pressure head and flow rate.
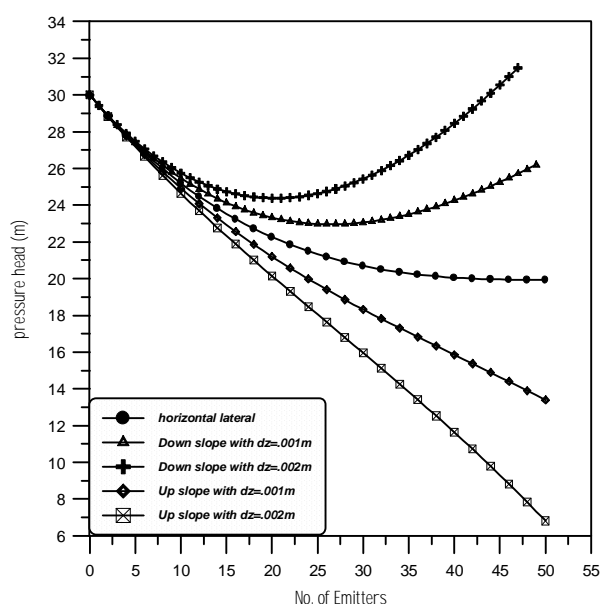

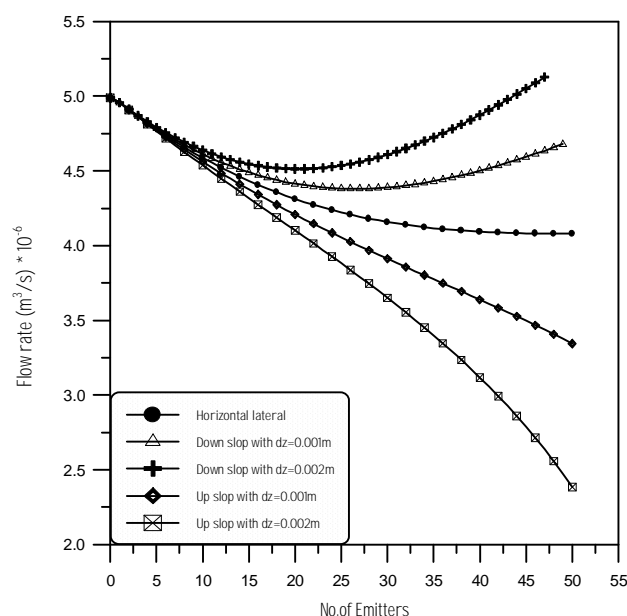**Figure (4). Effect of slope on pressure distribution along lateral.**

Figure (5). Effect of slope on flow rate distribution along lateral.

4.3. Effect of lateral length

Figure (6). shows the distribution of pressure head in the successive emitters along lateral for different values of length in which the pressure distribution computed for three different values of length (250 m, 350 m and 450 m) with corresponding Δx (space between two successive emitters) is (5 m, 7 m and 9 m). From this figure it can be seen that, the value of pressure

decreased with increasing the length due to increase in the friction losses. Therefore this parameter must be taken into consideration in design of the micro irrigation systems.

The distribution of flow rate along the lateral for different values of length is illustrated in Figure (7). The different lengths of laterals are equipped with the same number of emitters. From this figure one can find that, the flow rate decreased along lateral for the same length due to increasing the frictional losses. Also the flow rate decreased with increase the length of lateral due to the frictional losses.
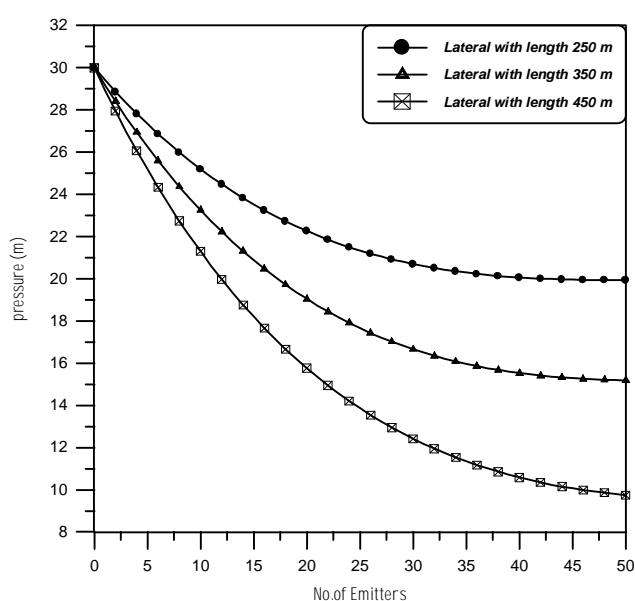

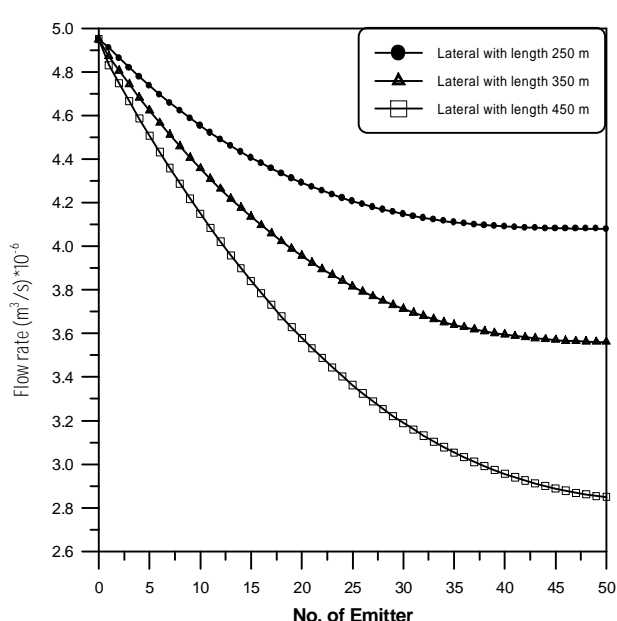**Figure (6). Effect of the lateral length on pressure distribution.**

Figure (7). Effect of lateral length on flow rate distribution.

4.4. Effect of flow velocity

Figure (8). shows the effect of the velocity of source on the design of lateral in which the pressure distribution computed for three different values of velocity (0.7 m/s, 1 m/s and 1.7 m/s).

From this figure it can be seen that, the pressure head decreased along lateral for the same value of velocity due to increase in the frictional losses with length. Also the pressure head decreased with the increase in the velocity of flow due to increasing the dynamic pressure losses.

The distribution of flow rate for different emitters along lateral for different values of velocity is illustrated in figure (9). From this figure it can be seen that, the flow rate for successive emitters decreased along lateral for the same velocity which is due to the decrease in

pressure head along lateral. It can be also noted that, the flow rate is decreased with increasing the velocity of flow due to the reduction in the pressure head.
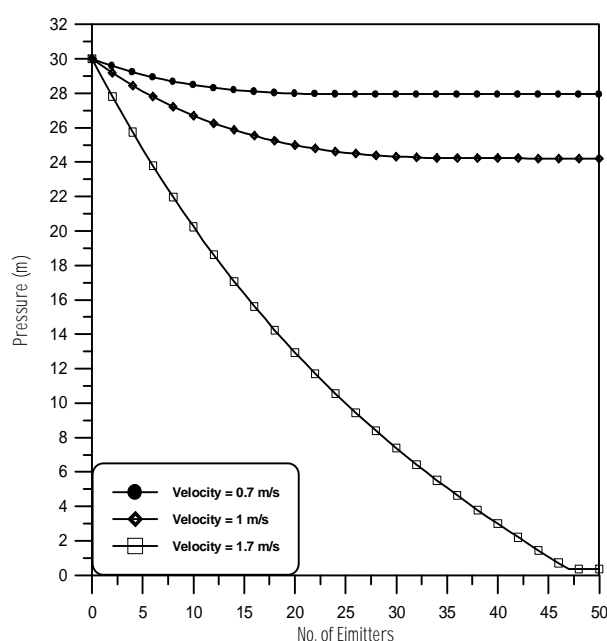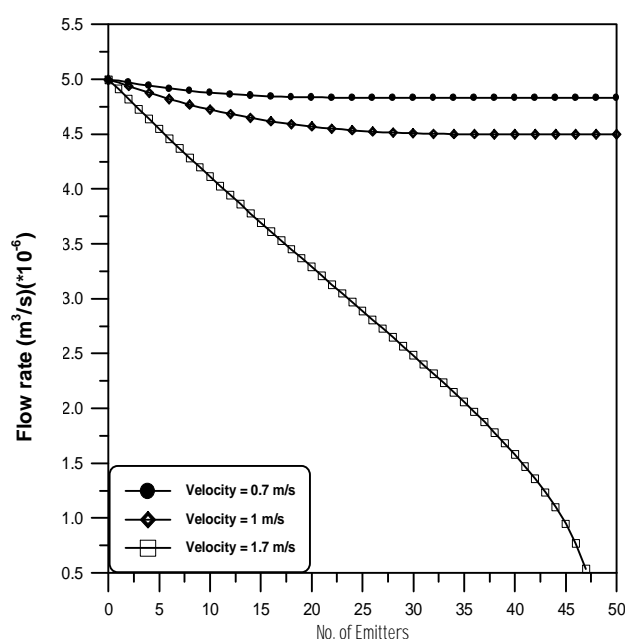

Figure (8).Effect of velocity on pressure distribution.

Figure(9). Effect of velocity on flow rate distribution.

5. Conclusions

In this paper the hydrodynamic characteristics of micro irrigation systems is numerically investigated using finite difference method and the effect of different design parameters such as (ground slope, length of lateral and velocity of flow) on the design of lateral. From the results obtained it can be concluded that:

The studied parameters have valuable effect on the hydrodynamic performance of micro irrigation systems. Since the small changes in these parameters caused large change in the distribution of the pressure and flow rate. Therefore the effect of these parameters must be taken into account in designing of micro irrigation systems and the optimum values of these parameters must be found and used in the design.

Also from the results obtained the FDM used is very accurate, efficient and simple compared with other methods used in literature and can be used accurately to design this type of irrigation systems.

34

6. References

[1] Wu, I. P., and Gitline, H. M., 1975, "Energy Gradient Line for Drip Irrigation Laterals", J. Irrig. Drain. Eng., 101(4), 323-326.

[2] Anyoji, H., and Wu, I. P., "Statistical Approach for Drip Lateral Design" Trans. ASAE, 30(1), 187-192, 1987.

[3] Warrick, A. W., and Yitayew, M., 1988, "Trickle Lateral Hydraulics I: Analytical Solution" J. Irrig. Drain. Eng., 114(2), 281-288.

[4] Yitayew, M., 1989,"Head Loss in Manifolds or Trickle Lateral: Simplified Approach "J. Irrig. Drain. Eng., 115(4), 739-743.

[5] Scaloppi ,E. J., and Allen R. G., 1993, "Hydraulics of Irrigation Laterals: Comparative Analysis "J. Irrig. Drain. Eng., 119(1), 91-115.

[6] [6] Hathoot, H. M., Al-Amoud, A.I., and Mohammad, F. S., 1993,"Analysis and Design of Trickle-Irrigation Laterals", J. Irrig. Drain. Eng., 119(5), 756-767.

[7] Kang,Y., and Nishiyama, S., 1996, " Analysis and Design Micro Irrigation Lateral" J. Irrig. Drain. Eng., 122(2), 75-82.

[8] Valiantas ,J. D., 1998,"Analytical Approach for Direct Drip Lateral Hydraulic Calculation" J. Irrig. Drain. Eng., 124(6), 300-305.

[9] Vallesquino , p., and Luque-Escamilla, P. L. , 2001,"New Algorithm for Hydraulic Calculation in Irrigation Laterals", J. Irrig. Drain. Eng., 127(4), 254-260.

[10] Valiantzas, j. D., 2002, "Hydraulic Analysis and Optimum Design of Multidiameter Irrigation Laterals" J. Irrig. Drain. Eng., 128(2), 78-86.

[11] Lakhdar ,Z. and Ahmed, K., 2002,"Numerical Methods of Micro Irrigation Lateral Design", Biotechnology Agron. Soc. Environ., 6(4), 231-235.

[12] Vedat, D., Husseyin, Y., Adnan, D., 2004,"Development of a Mathematical Model Using Dimensional Analysis for Predicting The Friction Losses in Drip Irrigation Laterals with Cyliderical Type in − Line Emitters", Turk. J. Agric. , 28, 101-107.

[13] Lakhdar, Z., Ahmad, K., Gerard, C., 2006,"Design of a Micro-Irrigation System Based on The Control Volume Method", Biotechnol. Agron. Soc. Environ. 10(3), 163 − 171.

[14] Gurol Yildirim   and Necati Agiralioglu, 2004,"Linear Solution for Hydraulic Analysis of Tapered Micro Irrigation laterals", Journal of Irrigation and Drainage Engineering, ASCE.

[15] Dale ,A. ,Anderson, John ,C. T., and Richard, H. P., 1984,"Computational Fluid Mechanics and Heat Transfer", McGraw- Hill Book Company.

7. Nomenclature

Symbol	Description
A	Cross – sectional area, m^2
C	Emitter coefficient
D	Lateral diameter, m
E	Energy head,m
g	Gravitational acceleration, m / s^2
H	Pressure head, m
hf	Losses head ,m
Q	Discharge , m^3 / s
Re	Reynolds number
v	Velocity, m / s
y	Emitter exponent
Z	Elevation ,m
μ	Viscosity ,m^2/s

Active Brazing of Tantalum – to – Tantalum

Nashwa A. A. Sa'ad

Baghdad Institute of Technology

F. A. Hashim

Mechanical Engineering Department College of Engineering Thi-Qar University

R. K Salim

Welding Engineering Department Technical College – Baghdad .

Abstract

The aim of this study is to start a work about the bonding mechanism of tantalum -to-tantalum brazed by active filler metal alloy which basely stand on using copper or silver with active element such as titanium. Brazing will happen under inert gas (argon). Ag4Wt% Ti,Cu8wt%Ti , and the eutectic Ag 26wt% Cu 4 wt % Ti are the active filler metal which are used , and the bonding phases at the filler metal / tantalum interface line almost contain (Ti Ta_2O_7) and ($Ti_{0.51}$ $Ta_{0.49}$ O_2) . Which means that active element (titanium) shares oxygen with tantalum to make this bond as a cheap filler .

لحام المونة الفعال للتتاليوم

المستخلص

ان هدف هذه الدراسة هو البدء في معرفة الية الربط لوصلة لحام التنتاليوم باستخدام سبيكة المونة الفعالة والتي تعتمد على عناصر مثل النحاس ، الفضة والعنصر الفعال (التيتانيوم) . يجري اللحام بالمونة في ظروف خاملة باستخدام غاز الاركون . المونة المستخدمة هي الفضة مع نسبة وزنية 4% من التيتانيوم ، النحاس مع نسبة وزنية 8 % من التيتانيوم ، وايوتكتك الفضة والنحاس (Ag 26wt% Cu 4 wt % Ti) مع نسبة وزنية للتيتانيوم 4 % ، اما طور الربط فقد وجد بأنه دائما يكون على شكل (Ti Ta_2 O_7) أو ($Ti_{0.51}$ $Ta_{0.49}$ O_2) حيث ان التيتانيوم يتقاسم ارتباطه مع التنتاليوم مع الاوكسجين . وفي النهاية فأن هذه الوصلة تعتبر قليلة الكلفة .

1. Introduction

From literature survey between 1960 to 1997 as shown in Table (1) [1 − 6] it was pointed that , refractory metals didn't have the data base that exists in the literature . Because of specific details on brazing equipment , such as vacuum levels , type of vacuum equipment , quality of inert gases and heat brazing cycles are not reported in most of the development work on the refractory metals [5] . Tantalum can be brazed with nickel-base filler metals , such as (Ni-Cr-Si) alloys . However , tantalum and nickel form brittle intermetallic compounds , such as (Ni_2Ta) in brazed joint [1 , 2 , 3] . In 1985 F.M Hosking studied sodium compatibility of refractory metal alloys – to – A ISI 304L stainless steel joint [7] . He brazed (Mo , Re , Ta , and W) alloy to AISI 304L stainless steel with nickel base filler metal in two forms (metallic glass and powder) by vacuum furnace . Silver – copper filler metals can produce joints with useful strength at room temperature [8] . The active-metal modifications (Ti additions) to (Ag – Cu) and (Au – Ni) alloys may be useful for tantalum joining particularly if residual oxide on the surface presents a wetting problem [5] .

Ta – V – Ti and Ta – V – Cb alloys given in Table (2) [3] , may be suitable for certain high temperature applications . Brazing should be done in vaccum of 10^{-4} torr or better , but there is affinity to vaporize titanium and vanadium from molten filler metal during the brazing cycle because of their high vapor pressure [3] . Also pure titanium and titanium alloys might be suitable for brazing tantalum . 1n 1977 , Scientific Oak Ridge National Laboratory (ORNL) has been instrumental in the development of brazing filler metals for applications at temperature above (1000 ˙C) [6] . The filler metals and brazing temperatures employed in the development of these alloys are presented in Table (3) [6] . They used tantalum as refractory , aluminum oxide samples as ceramic were bonded with vacuum of 10^{-6} torr . The excellent flowability of these alloys on tantalum was recorded . The aim of this study is to recognize the Ta – to – Ta joint characteristics by usual brazing filler containing titanium depending on optical micros copying (OM) , and X-ray diffraction (XRD) testing .

Table (1). Filler metals used in tantalum brazing between 1960 to 1997[1-6].

Filler Metal	Service Temperature (°C)	The References
Nickel – Base		
Ni-Cr-Si alloys	981 ≥	[1,2,3]
Copper –Base		
Cu-Au	Low Temperature	[4,1,2,3]
Cu-Sn	Not Specified	[3]
Cu-Ti	Not Specified	[3]
Silver –Base		
Ag-Cu	Room Temperature	[3]
Ag-Cu-Ti	Not Specified	[5]
Gold –Base		
Au-Ni	Low Temperature	[5,1]
Au-Ni-Ti	Not Specified	[5]
Au-Cu	Low Temperature	[5,1]
Tantalum –Base		
Ta-V-Ti	1482 ≥	[5,3]
Ta-V-Nb	1482 ≥	[5,3]
Titanium-Base		
Pure Ti	Not Specified	[2]
Ti-Cr	1927 ≥	[3]
Ti-V	Not Specified	[5]
Ti-V-Be	1927 ≥	[3]
Ti-Zr-Be	Not Specified	[2]
Ti-V-Cr	1000 <	[6]
Ti-Zr-Ge	1000 <	[6]
Ti-Zr-Ta	1000 <	[6]
Ti-Zr-Nb	1000 <	[6]
Ti-Zr-Cr	1000 <	[6]
Ti-Zr-B	1000 <	[6]
Ti-V –Nb	1000 <	[6]
Ti- V-Mo	1000 <	[6]
8-Platinum-Base		
Pure platinum	Not Specified	[2]
Pt-Ir	Not Specified	[2]
Pt-Rh	Not Specified	[2]
9-Zirconium-Base		
Zr-Nb-Be	Not Specified	[2]
Zr-Ti-V	Not Specified	[5]
10-Palladium-base		
Pure Palladium	Not Specified	[2]

Table (2). Typical brazing filler metal for tantalum alloys for service temperature up to 1482cº [3].

Filler metal composition weight percent	Temperature (°C)	
	Brazing	Remelt
10Ta-40V-50Ti	1760	2381.10
20-Ta-50V-30Ti	1760	2381.10
25Ta-55V-20Ti	1825.5	2204.40
30Ta-65V-5Ti	1825.5	2381.10
5Ta-65V-30Nb	1815.6	2281.11
25Ta-50V-25Nb	1871.1	2481.90
30Ta-65Vv-5Nb	1871.1	2281.11
30Ta-40V-30Nb	1926.7	1981.90

Table (3) .Ternary system in which filler metal have been developed and their recommended applications [6].

Filler Metal System	Approximate Brazing Temperature (°C)	Materials		
		Refractory metals	Graphite	Al $_2$ O$_3$
Ti-V-Cr	1550-1650	X (a)	X	X
Ti-Zr-Ta	1650-2100	X	X	-
Ti-Zr-Ge	1300-1600	X	X	-
Ti-Zr-Nb	1600-1700	X	X	-
Ti-Zr-Cr	1250-1450	X	- (b)	-
Ti-Zr-B	1400-1600	X	-	-
Ti-V-Nb	1650	X	-	-
Ti-V-Mo	1650	X	-	-

(a) (X) =Applicable for joining .
(b) (-) = Not applicable for joining .

2. Experimental Work

A 0.15 mm sheet thickness of pure tantalum manufactured by Pansee Metalwork Gmblt was used as a base metal in this work . High purity powders of copper , silver , and titanium metals were used to prepare the active paste filler metal alloy . The paste prepared by manual mixing

(for one minute) , the suitable mass of filler with about (0.5 mm^3) of glycerin and   (1 mm^3) of alcohol ethanel to form the paste , which is suitable for one butt joint assembly . The suitable gap size is about 0.1 mm , and the overall mass is about 0.6 gram , which was used for all testing samples . The dimension of tantalum samples are 25 x 25 x 0.15 mm . More than nine tantalum to tantalum butt joint assembly were used , the joining process done by three fillers , metal alloy types ; Ag4wt%Ti (Ag4Ti) , Cu 8 wt%Ti (Cu 8Ti) , and eutectic Ag 26 wt%Cu4wt% Ti . (AgCuTi) . For each filler, three joint assembles were carried out , one joint for microstructure testing , and the others for X-ray diffraction testing . Furnace brazing with argon , as a protection gas used to complete the brazing process . A muffle furnace type with a controlled-argon-atmosphere is prepared with gas flow rate of about 1-3 L/min in a stainless steel retort . The brazing temperatures are , 950 $^\circ$C , 1050 , and 1100 $^\circ$C for the fillers AgCuTi , Ag4Ti , and Cu8Ti respectively . The holding time at brazing temperature is about five minutes . Grinding and polishing processes were carried out to prepare the microstructure testing samples , while the broken samples at the bonding interface will be used for XRD testing after grinding process to the two broken sides , to be examined by Philips-PW1840 X-ray diffractometer . The X-ray tube target was copper (λ for Cukα = 1.5405 A$^\circ$) , the filter is nickel . The 20 ranges taken was from 10° – 90°, in the speed of 3 degree/min . Identification of phases was based on matching with powder diffraction files (JCPDS) [9] . The welded samples are fixed by simple two plates of molybdenum (50 x 50 x 0.25 mm) with two screws to maintain the joint in proper dimensions .

3. Results and discussion

Optical micrographs for a cross section brazed by Ag4Ti filler metals in Figure (1) show mutual dissolution of tantalum and filler metal in a wave form . This may be explained by the solubility of B-Ti in tantalum [9] . Closer scrutiny revealed formation of a distinct layer adjacent to the base metal and migration of separated particles from this layer to central region of filler metal as in Figure (2) . This morphology may represent the aggression and disruption of the bonding layer by active filler metal . Also dark points were observed in the braze joint , this may refer to the titanium oxide formation duo to the bonding mechanism by active filler metal alloy [10,11] .

The XRD results for Ta to Ta assemblies brazed by Ag4Ti as in Figure (3) show that ; the bonding phases are (Ti Ta$_2$ O$_7$) and (Ti$_{0.51}$ Ta$_{0.49}$ O$_2$) , which refer to the oxide layer at the surface of tantalum , and the bond created by the action of tantalum sharing its passivity oxide

film before combined with titanium [12] . The presence of Ag and Ti phases referes to (Ta-Ti) solid solution . While the separated phases of Ti and Ta refer to the limited solubility of Tantalum in B-Ti and tend to formation of intermelallic phases .

   The brazing of Ta to Ta with silver – 4wt% Ti filler metal alloy results in an improved joining with low cost as compared with that brazed by expensive filler metal as in Tables 2 and 3 and part of Table (1) .
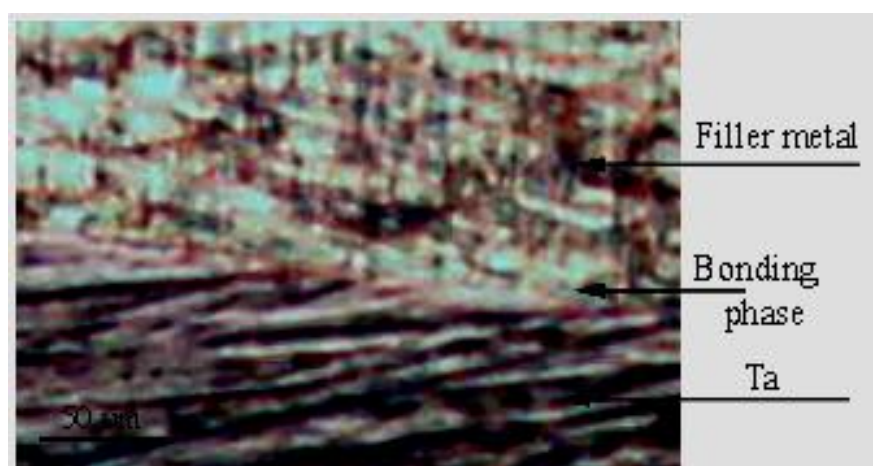

Figure (1) .Optical micrograph for (Ta – to – Ta) assembly brazed by Ag4Ti filler metal .

   Figure (4) shows the optical micrographs for Ta – to Ta joint which was brazed by Cu 8 Ti , in which a mutual dissolution of tantalum and active filler metal was remarked as a waved interface like what was happened with the joint by Ag 4 Ti . However the bonding mechanism completed by the existing of Ti Ta$_2$ O$_7$ phase only as shown in Figure (5) .

   Using of eutectic AgCuTi filler metal alloy to braze Ta – to – Ta joint results in a good joining . Optical micrographs for AgCuTi filler / tantalum interface as in Figure (6) , shows a formation of a distinct layer adjacent to base metal . This layer has expanses in roots form , were expanded in eutectic braze metal as in figure 6 – a . This may refer to the formation of more than one bonding phase . The closer scruting of interface line shows separation part of roots and many particles from bonding phase . This morphology may represent the dissolution or erosion of tantalum by active filler . The XRD chart for this joint Figure(7) shows that the bonding phases are ; Ti Ta2 O7 , Ti $_{0.51}$ Ta $_{0.4}$, O$_2$, Ti Ta$_{13}$ O$_{47}$, and Ti O phase . The last phase explains the good bonding structure which means that the active element (titanium) forms a good bonding layer [11] .

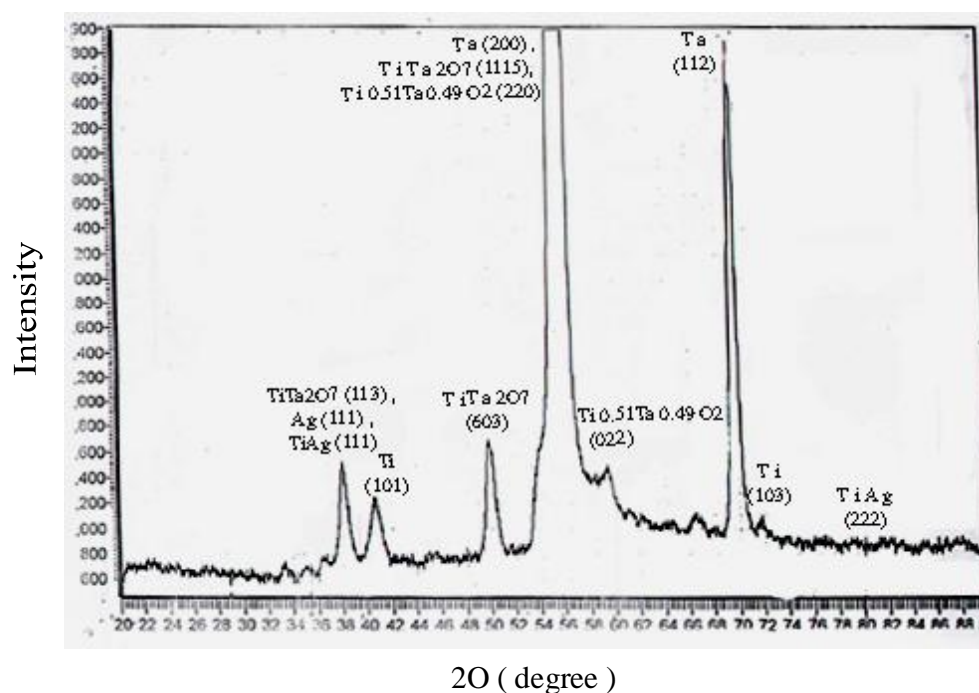**Figure (2) . (Ta – to - Ta) assembly brazed by Ag4Ti filler metal .**

2O (degree)

Figure (3) . X-ray diffraction chart for (Ta – to – Ta) assembly brazed by Ag4Ti filler metal .

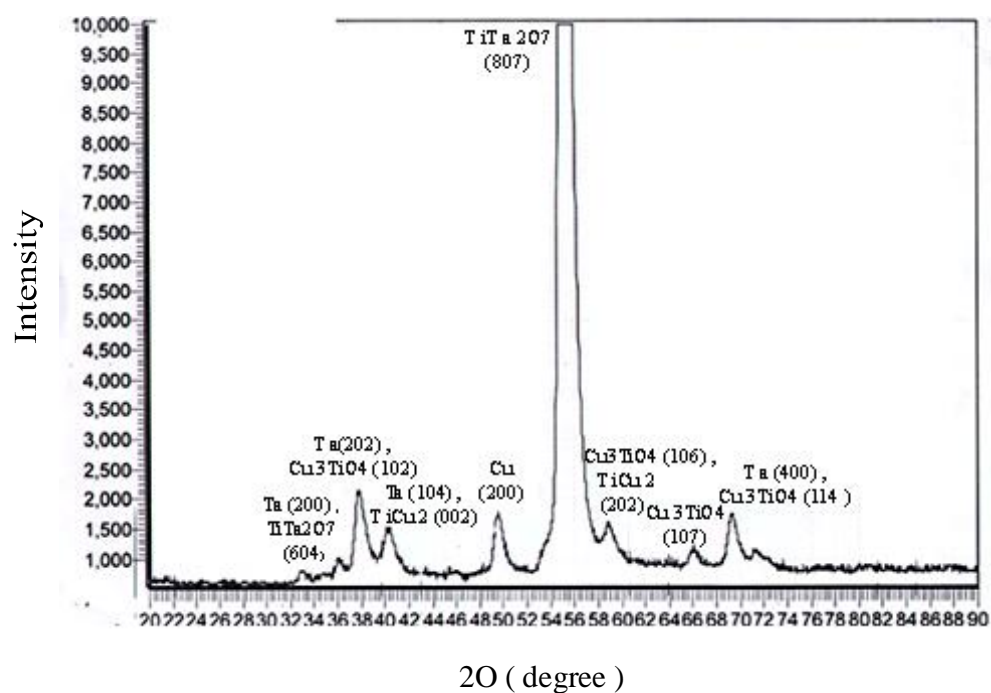**Figure (4). Interface of (Ta –Ta) assembly brazed by Cu^Ti filler metal.**

2O (degree)

Figure (5) . X- ray diffraction chart of (Ta – to – Ta)

assembly brazed by Cu8Ti filler metal.
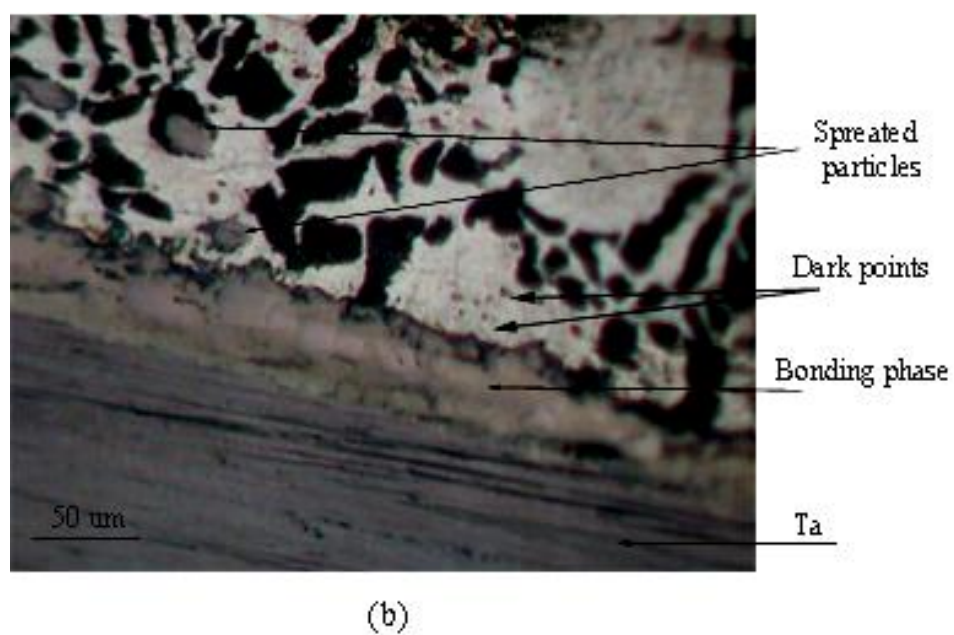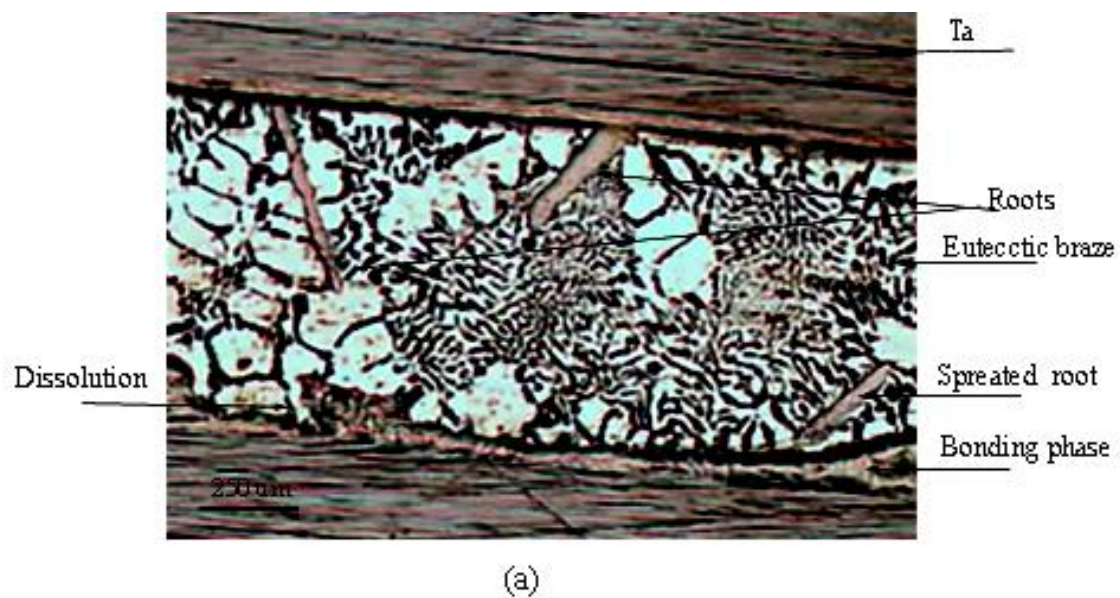
(a)

(b)

Figure (6). (a and b) Represents optical micrographs for (Ta – to – Ta) assembly brazed by eutectic AgCuTi filler metal .
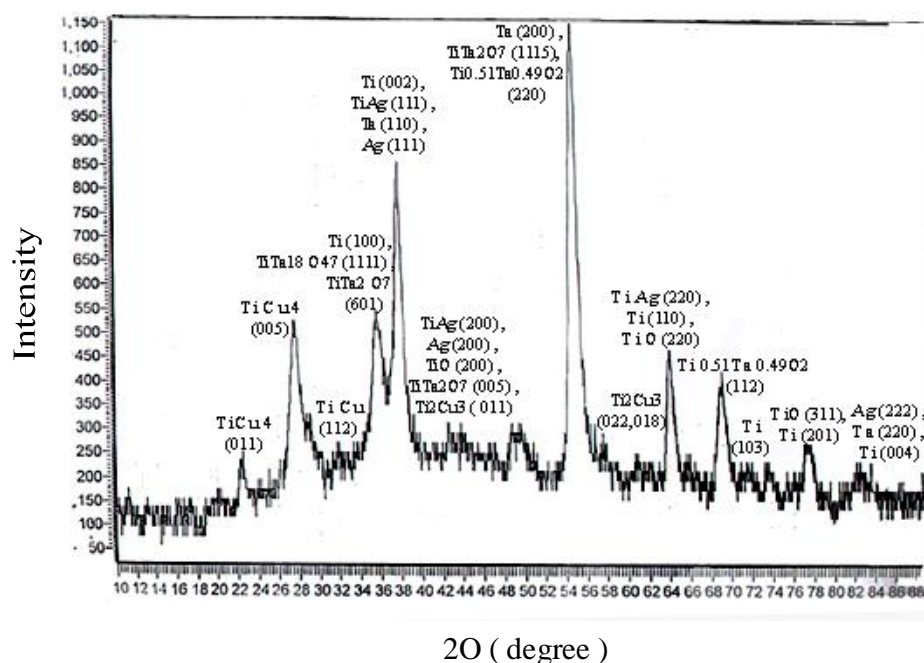
**Figure (7) . X- ray diffraction chart for (Ta – to – Ta)
assembly brazed by eutectic AgCuTi filler metal .**

4. Conclusions

1. The Tantalum to tantalum brazed assembly by Ag4Ti exhibits good joining with aggression of tantalum and dark point were observed in brazed region .

2. The Tantalum to tantalum brazed assembly by Cu8Ti exhibits additional improvement in joining with low cost as compounded with high active filer metal alloy .

3. The bonding phases in most assemblies brazed by CuTi , AgTi and AgCuTi filler metal are $TiTa_2O_7$ and $Ti0.51\ Ta_{0.49}O_2$ with good interface bonding layer with TiO for using autectic filler metal alloy .

5. References

[1] AWS , 1975 ," Brazing Manual " , Third Edition , American Welding Society Inc..

[2] AWS , 1978 , " Welding Hand Book " , 7th Edition , Vol. 2 .

[3] AWS , 1984 ," Welding Hand Book " , Metal And Their Weldability " , 7th Edition , Vol. 4 .

[4] AWS , 1960 , " Brazing Manual " , Third Printing , London ,Chapman and Hall Ltd .

[5] ASM , 1997 , " Hand Book of Welding , Brazing and Soldering " .

[6] Canonico, D. A. and Slaughter, G. M., August 1977 ," Direct Brazing of Ceramics , Graphite and Refreactory Metals " , Welding Journal .

[7] Hosking, F. M., July 1985 ," Sodium Compatibility of Refractory Metal Alloy-Type AISI 304L stainless Steel Joint " , Welding Journal .

[8] Vanco, P. T. and Hosking, F. M., October 2002 , " Aging of Brazed Joints interface Reactions in Base Metal / Filler Metal " ,Part 1 , Welding Journal .

[9] International Center for Powder Diffraction Data , 1985 ," Joint Committee of Powder Diffraction Standard , (JCPDS) – Powder Diffraction File , Alpha Betical / Index-Inorganic Phases " , Pennsylvania , USA .

[10] Max Hansen , April , 1998 ," Constituation of Binary Alloys " , Second Edition , Mcgraw Hill Book Company , London .

[11] Fadhel, A. H., 2003 ," Microstructural and Bonding Mechanism of Activity Brazed Ceramic / Ceramic System " , PhD Thesis , University of Technology , Iraq .

[12] Al-Rubaii , A. O. J., 2007 ," Properties and Mechanism of Ceramic (Al_2O_3) / Metal (Cu) Bonding , PhD Thesis , University of Babylon , Iraq.

[13] Bever, M. B., 1986 , " Encyclopedia of Materials Science and Engineering " , MIT , USA , Vol.7 , Great Britain and Co. Ltd . Exeter .

Spectrum Analysis of The Gate of Dike Structure Under Nonstationary Random Loading

Kadhim Karim Mohsen

Mechanical Engineering Department
College of Engineering
Thi-Qar University

Abstract

This paper investigates the nonstationary random excitations with a constraint on mean square value such that the response variance of a given linear system is minimized. It is also possible to incorporate the dominant input frequency into the analysis. The excitation is taken to be the product of a deterministic enveloping function and a zero mean Gaussian nonstationary random process. The power spectral density function of this process is determined such that the response variance is minimized. The numerical results are presented for multi-degree freedom system and modeled to predict the behavior of the gate of dike Structure under random water loading.

Keywords : Random loading ,seismic excitation, no stationary process .

التحليل الطيفي لبوابة السدود المائية المعرضة الى احمال عشوائية غير مستقرة

المستخلص

تم في هذا البحث در اسة الاثارة الناتجة عن الاحمال العشوائية غير المستقرة لنظام خطي مع معدل مربع القيمة للاحمال لغرض تصغير المعيارية لاستجابة النظام . كما تم استخدام مدخلات مجال التردد ضمن التحليل , مع الاخذ بنظر الاعتبار حاصل ضرب الدالة المحددة والمعدل الصفري لعملية نوع(كاوشين) العشوائية غير المستقرة حيث تم ايجاد كثافة طيف القدرة لتصغير الاستجابة المعيارية للنظام . النتائج العددية التي تم عرضها في هذا البحث للانظمة المتعددة درجات الحرية تم الاستفادة منها للتنبوء بسلوك هيكل بوابة السدود المائية المعرضة الى احمال عشوائية غير مستقرة .

1. Introduction

The analysis of flow through earth dams typically proceeds deterministically and results sometimes be quite misleading. In fact it is well known that water permeability varies randomly and spatially from point to point in space and an improved earth dam model should incorporate this variability. Stationary random field follows a lognormal distribution with prescribed mean, variance, and spatial correlation structure. The mean and variance of the total flow rate through the dam and free surface drawdown are estimated. Dikes (also known as flood gates or levees) shown in Figure(1). are used to manage or prevent water flow into specific land region, while other structures such as a dam is a barrier that impounds water or underground streams. Dikes generally serve the primary purpose of retaining waters. Hydropower and pumped-storage hydroelectricity are often used in conjunction with dikes to provide clean electricity for millions of consumers [1].

Surface topography as a nonstationary random process is often considered as a narrow bandwidth of features covering the form or shape of the surface. The study of many measurements as well as the possibility of a dominant range of features there is always an underlying random structure where undulations in surface height continue over as broad a bandwidth as the surface size will allow [2]. Many physical effects each confined to a specific waveband but no band being dominant. By invoking the central limit theorem and applying through Gaussian statistics that the variance of the height distribution of such a structure is linearly related to the length of the sample involved. In another form, the power spectral density, this relationship is shown to agree well with measurements of structures taken over many scales of size, and from throughout the physical universe. [3]. Spectral and auto correlation analysis techniques can be employed for a linear zed structure model to determine the random characteristics of structure (elongation, dynamic loads, stress). Items of interest include the peak values, RMS values, probability of exceeding a particular level or range, dominating frequencies, and further study of cumulative damage of components [4, 5].

The dynamic stiffness method applies mainly to excitations of harmonic nodal forces. For distributed loads, modal analysis is generally required. If the distributed load is adequately represented, explicit exact solutions will be found. A structure with members having distributed loads can be analyzed by two systems: one is associated with the individual members having distributed loads and the other is associated with resulting equivalent nodal forces. The required

frequency functions are given for all possible cases. Contact area by taking local, weighted spatial average to account for the distributed contact [6]. Statistical properties such as power spectral density, autocorrelation function and variance of the induced spatial excitation are related to the counterparts of the original random field. It was found that the distributed contact acts like a low-pass filter whose bandwidth is governed by the contact interface and the weight function [7, 8].
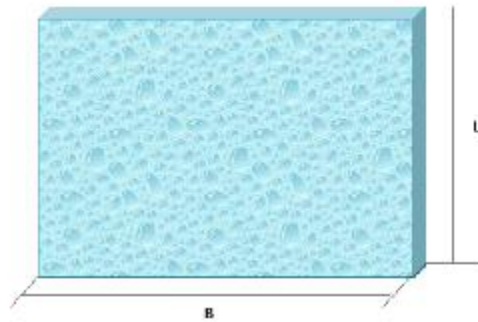

Figure (1) .Dike .

2. Analysis procedure

The input is modeled as a nonstationary random process

$$q(t) \;=\; \mathcal{U}(t)\mathcal{W}(t) \tag{1}$$

Where $\mathcal{W}(t)$ = a Gaussian nonstationary random process with zero mean and known variance; and $\mathcal{U}(t)$= a known modulating function.

$\mathcal{U}(t)$ is taken as [9]

$$\mathcal{U}(t) = e^{-\beta t} - e^{-\gamma t} \tag{2}$$

where β and γ = parameters of modulating function.

The autocorrelation of the response of a time invariant system is given by:

$$R_x(t_1, t_2) = \int_0^{t_1}\!\!\int_0^{t_2} \mathcal{U}(\tau_1)\mathcal{U}(\tau_2)R_{\mathcal{W}}(\tau_2 - \tau_1)h(t_1 - \tau_1)h(t_2 - \tau_2)d\tau_1 d\tau_2 \tag{3}$$

 Where h (t) is the impulse response function, τ time delay.

Since $\mathcal{W}$ is a nonstationary process, its autocorrelation can be expressed as:

$$R_W(\tau) = \int_0^\infty S\,(\Omega)\,cos\Omega\tau d\Omega \tag{4}$$

where $S\,(\Omega)$ is the spectrum function of the excitation Ω. Thus the response variance can be written :

$$\sigma^2(t) = \int_0^\infty S\,(\Omega)H(\Omega,t)\,d\Omega \tag{5}$$

Here H $(\Omega,$ t) ensembles a time-varying frequency response function.

The mean value of the spectrum excitation is defined as

$$E = \int_0^\infty S\,(\Omega)d\Omega \tag{6}$$

Using Fourier transform pair (Winer-Khintchine relation) [10] yields

$$R\,(\tau) = \int_0^\infty E\,\omega(t)dt \tag{7}$$

 Where $\omega(t)$ = natural frequency of the system.

Expanding Equation (7) in the series :

$$R\,(\tau) = \sum_{i=1}^\infty E_i + \omega_i(t) \tag{8}$$

A particular solution is obtained by expanding the real function $S\,(\Omega)$ in the series

$$\sigma(S) = \sum_{i=1}^\infty A_i\phi_i\,(\Omega) \tag{9}$$

Where $\sigma(S)$ = the standard deviation of spectrum.

$\phi_i\,(i\,=\,1,2,\dots)$ = set of orthonormal functions such that

$$\int_0^\infty \phi_i\phi_j\,d\Omega = 0 \quad ; i \neq j \tag{10a}$$

$$\int_0^\infty \phi_i\phi_j\,d\Omega = 1 \quad ; i = j \tag{10b}$$

After using Lagrangian multiplier $\Pi(t)$, and combining Eq.8 with Eq. 9 for minimization

$$L[A_1, A_2, A_3 \dots, \Pi(t)] = \int_0^\infty \sum_{i=1}^\infty (\phi_i \phi_j)^2 H(\Omega, t) d\Omega - \omega(t) \sum A_i^2 - E \tag{11}$$

For $\dfrac{\partial L}{\partial A_i} = 0 \ (i = 1,2,\dots)$ *and* $\dfrac{\partial L}{\partial \Pi} = 0$ **gives**

$$\sum_{i=1}^\infty A_i f_{ij}(t) - \omega(t) A_i^2 = 0; \qquad (j = 1,2,\dots) \tag{12}$$

Since $f_{ij}(t)$ is a time function

$$f_{ij}(t) = \int_0^\infty (\phi_i \phi_j)^2 H(\Omega, t) d\Omega \tag{13}$$

$$\sum_{i=1}^\infty A_i^2 = E \tag{14}$$

This is an algebraic eigenvalue problem that can be solved using standard techniques. Thus one can get the eigenvalues $\omega_i(t)$ (i = 1,2, …) and the corresponding eigenvectors $(A_{1i}, A_{2i},\dots)$ with the normalization condition of Eq. 12. Further, substitution of Eq, 12 in Eq. 5 and rearrangement leads to

$$\sigma^2(t) = \omega(t)E \tag{15}$$

This shows that while it is possible to get as many solutions as the number of terms in the expansion for the power spectral density function PSD, it is the smallest eigenvalue and the corresponding eigenvector that leads to the lowest response variance. This is true for every time instant t. For finding the critical excitation in a given interval of time, the above equations has to be repeated for every (i), the excitation leading to the minimum response is taken as the desired solution.

Generalized model

General equation of motion for time invariant system

$$\ddot{q}_i + 2\zeta_i \omega_i \dot{q}_i + \omega_i^2 q = \mathcal{U}(t)\mathcal{W}(t) \tag{16}$$

The displacement response variance of the ith mass of a multi degrees of freedom system system under the input of Eq. 1 is given by

$$\sigma_i^2(x, \Omega, t) = \int\limits_0^\infty S(x, \Omega, t) H_i(x, \Omega, t) d\Omega \tag{17}$$

For complex frequency response

$$H_i(x, \Omega, t)$$

$$= \int\limits_0^{t_1}\int\limits_0^{t_2} \sum_{k=1}^n \sum_{i=1}^n \Gamma_j \Gamma_k \phi_{ij} \phi_{ik} \mathcal{U}(\tau_1) \mathcal{U}(\tau_2) h_k(t_1 - \tau_1) \, h_k(t_2 - \tau_2) cos\Omega(\tau_2$$

$$- \tau_1) d\tau_1 d\tau_2 \tag{18}$$

$$h_k(t) = \omega_{dk}^{-1} e^{(-\zeta_k \omega_k t) sin\omega_{dk} t} \tag{19}$$

$$\omega_{dk} = \omega_k \sqrt{1 - \eta_k^2} \tag{20}$$

ω_{dk}=damped natural frequencies of the system, η_k =coefficients of viscous damping, Γ_j and ϕ_{ij}= the modal participation factors and mode shapes, respectively. The critical PSD function can be computed again as in the case of a SDOF system. However, here two important points have to be noted. First, for every level i one can get a different critical PSD function (S). Second, the critical PSD would vary depending on the response variable considered. Once the response variable is selected as to velocity, displacement, bending moment, shear etc., the computations are straightforward .The determination of the critical random input to the gate of the dike is considered as a model for the present paper. It is possible to solve the present problem in the time domain also. This involves the minimization of the response envelope in a given interval. The response envelope of response of the system governed by Eq. 16 is :

$$R(t) = 2 \int\limits_0^t [\mathcal{U}(t) \mathcal{W}(t) \dot{q}(t) - 2\eta\omega\dot{y}(t)] \dot{q}(t) dt \tag{21}$$

$\mathcal{W}(t)$ being a nonstationary random process, it can be expanded in a series as;

$$\mathcal{W}(t) = \sum_{i=0}^n D_i \, sin(\lambda_i t - \psi_i) \tag{22}$$

Here $D_i's$ are deterministic constants and $\psi_i's$ are independent random phase angles distributed uniformly in the interval (-π,π). Substituting Eq. 22 into Eq.21 and after some manipulation, one gets :

$$\mathbf{R}(t) = \sum_{k=1}^{n} \sum_{i=1}^{n} D_{ij} D_{ik} f_{ik}(t) \tag{23}$$

Here $f_{ij}(t)$ is a known function of time. The RMS constraint on the input can be expressed in terms of $\mathbf{D_i's}$ as

$$E = \sum_{i=1}^{\infty} D_i^2 \tag{24}$$

By substituting equations (18-24) into equation (17) and completing the integration by residue to obtain the variance of the gate of the dike :

$$\sigma_i^2(x,\Omega,t) = \sum_{j=1}^{n} \sum_{k=1}^{n} \sum_{i=1}^{n} \Gamma_j \Gamma_k \phi_{ij} \phi_{ik} \mathcal{U}(\tau_1) \mathcal{U}(\tau_2) D_{ij} D_{ik} sin(\lambda_i t - \phi_{ij}^2 \phi_{ik}^2) \tag{25}$$

The angular natural frequencies λ_i and Eigen functions are :

$$\lambda_i = \left(\frac{\mathcal{Z}_i}{\ell}\right) \sqrt{\frac{G}{\rho}} \tag{26}$$

$$\phi_{ij}(\mathbf{x}) = \frac{2 \mathbf{J_o}\left(\frac{\mathcal{Z}_i(\mathbf{x})}{\ell}\right)}{\mathcal{Z}_i \mathbf{J_1}(\mathcal{Z}_i)} \tag{27}$$

Here Jo and J_1 are the Bessel's function of the first kind. $\mathcal{Z}_i's$ refers to the zeros of Jo. The variance of the gate of the dike relative to the random water loading .

3. Results and discussion

A gate of water dike $\ell = 44.6\,m$ in height with a rectangular cross section under nonstationary random loading shown in Figure (2). is considered and subjected to random vibration of water. It is required to find the critical outputs such that the lateral displacement variance. The material properties of the dike are taken as density $\rho = 3 \times 10^5$ kN/m^3; viscous damping coefficient $\eta = 0.2$; and shear modulus G= 2.92×10^6 kN/m^2.
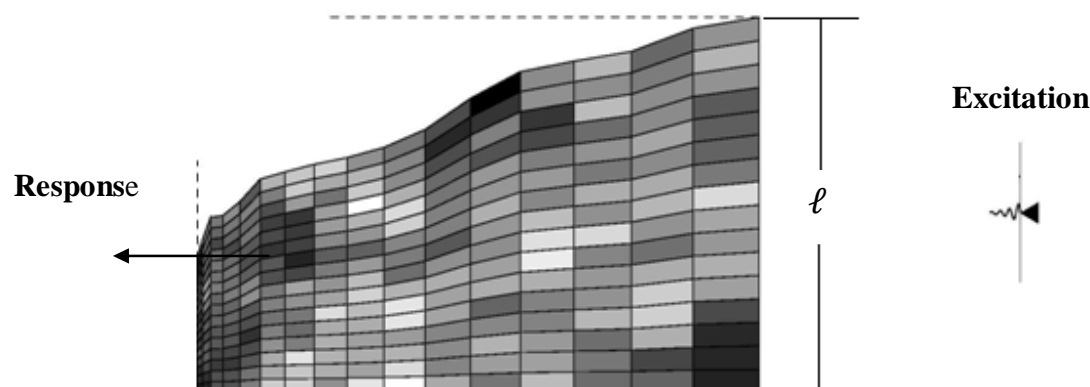
Figure (2). Systematic representation of the gate of the dike .

The numerical values of the critical outputs variance of the gate of dike can be tabulated as shown in Table (1).

Table (1). Critical outputs variance for the gate of dike .

index	λ_i/E (sec')	$\mathcal{Z}_i$	$\Gamma_j\Gamma_k$	$\sigma^2(x, \Omega, t)$
1	0.6032×10^{-4}	2.4048	0.85	9.6
2	0.7321×10^{-4}	5.5201	1.01	1.03
3	0.3216×10^{-4}	8.6537	1.65	0.56
4	0.2444×10^{-4}	11.7915	1.99	0.57
5	0.2301×10^{-4}	14.5032	2.01	0.5
6	0.2202×10^{-4}	14.8476	3.66	0.46
7	0.2121×10^{-4}	15.7654	4.16	0.14

The modal solution natural frequencies and mode shapes are needed to calculate the spectrum solution by applying nonstationary random excitation shown in Figure (3). The dynamic characteristics of the structure, such as the standard deviation of response are computed as shown in Figure (4).

The power spectral density shown in Figure (5). was evaluated in order to find the displacement response variance of dikes gate. Nastratn program version 4.4 was used to analyze

the mode shapes of the gate of the dike shown in Figures (6-9) to obtain the natural frequencies which can be used to evaluate the variance of the response of the gate Figure (10)

The advantage of the solution in time domain is at all the desired frequencies can be included explicitly in the input. The details of this time domain solution are being currently studied in the paper. In the present method it should be noted that one does not arrive at a unique time history of excitation, but instead an ensemble of time functions forming a stochastic process is obtained.

Critical excitations as developed here are by definition system dependent. This would lead to different critical inputs for different types of dike's gate structures. This naturally is a limitation. To circumvent this difficulty one can find the critical input for the most important structure and use this to arrive at the critical excitation that is specification dependent, but is inde-pendent of the structures to be built.
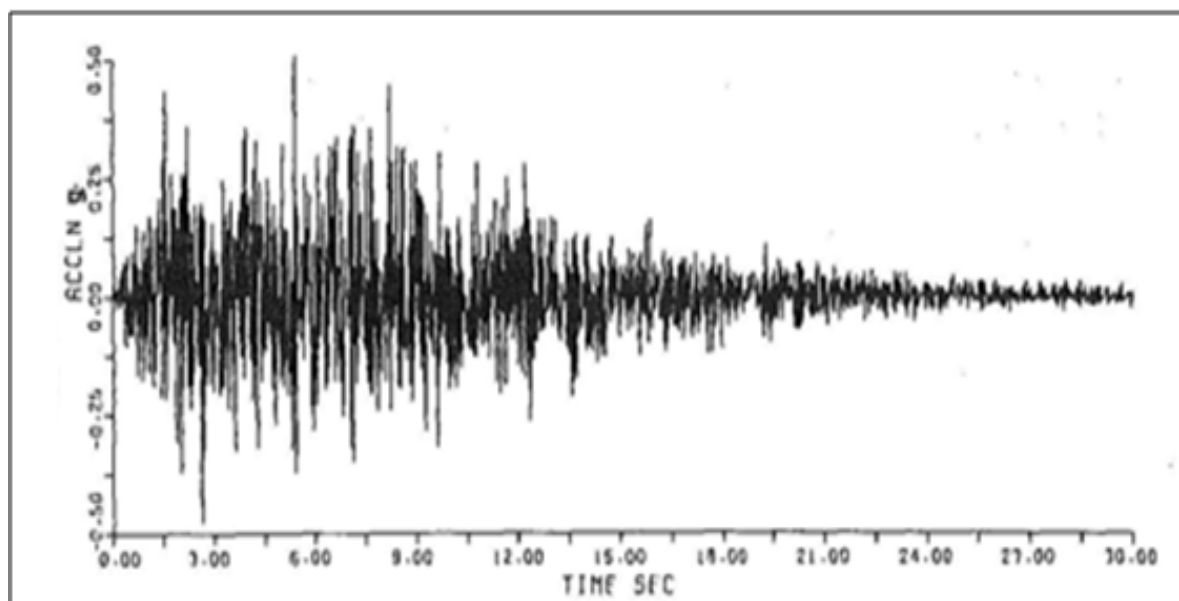

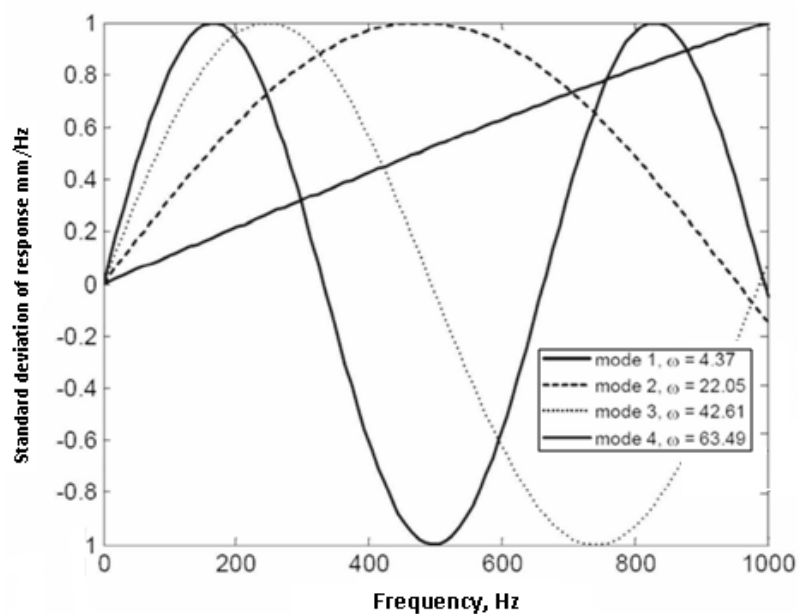**Figure (3) . Nonstationary Gaussian random excitation**.

Figure (4). Standard deviation of response for the four modes of the gate of dike.
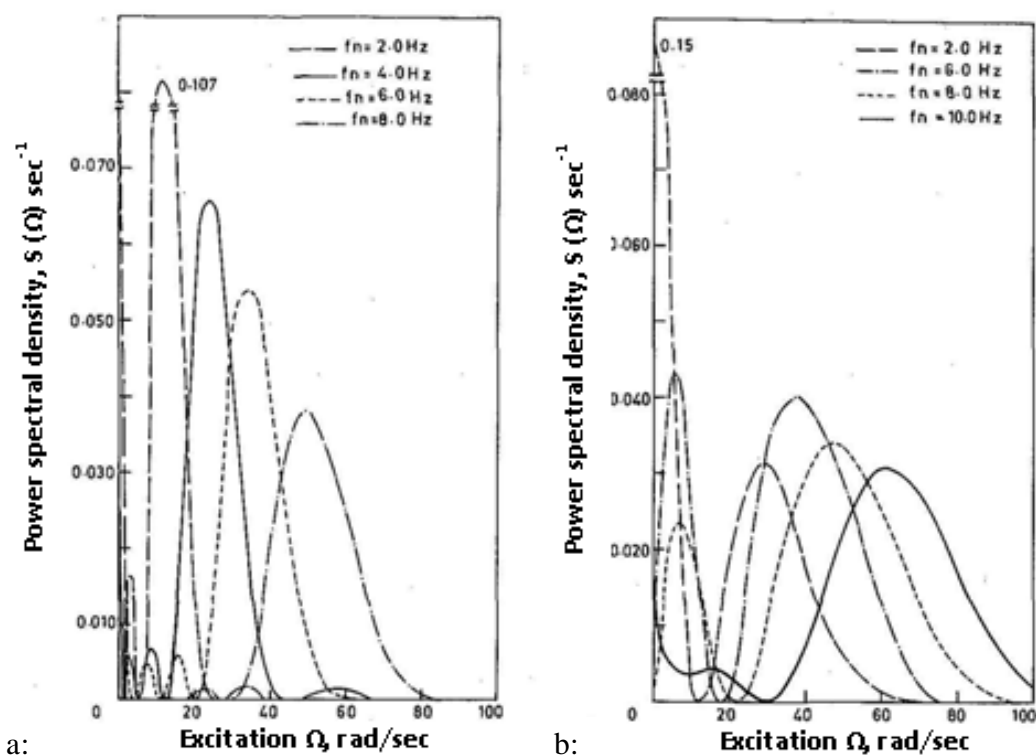

a:

b:

Figure (5). Critical spectrum functions for different natural frequencies of the gate of the dike
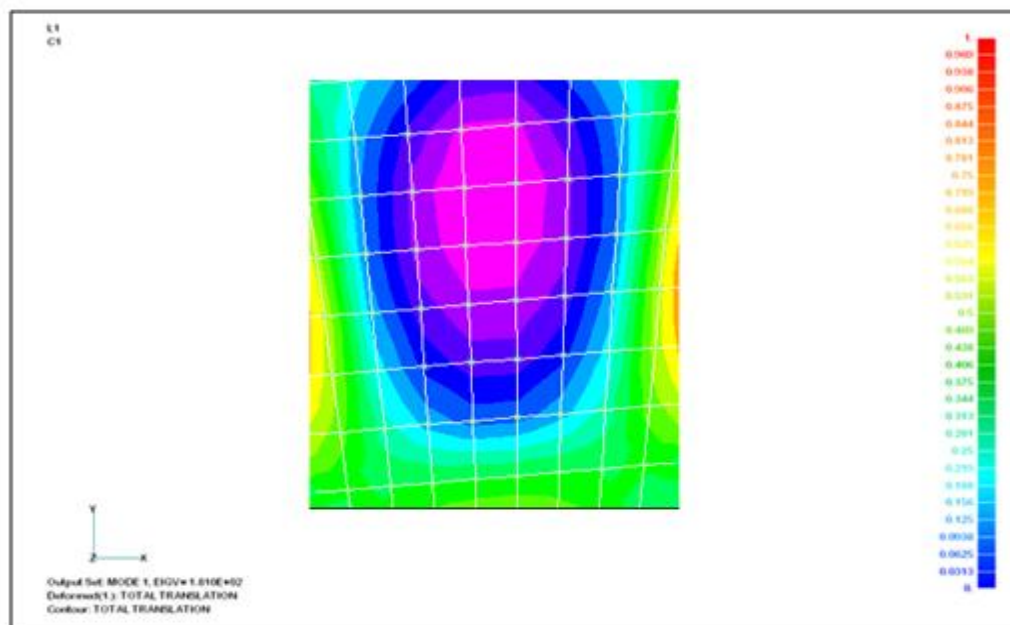**(a) In terms of exponentials. (b) In terms of polynomials .**

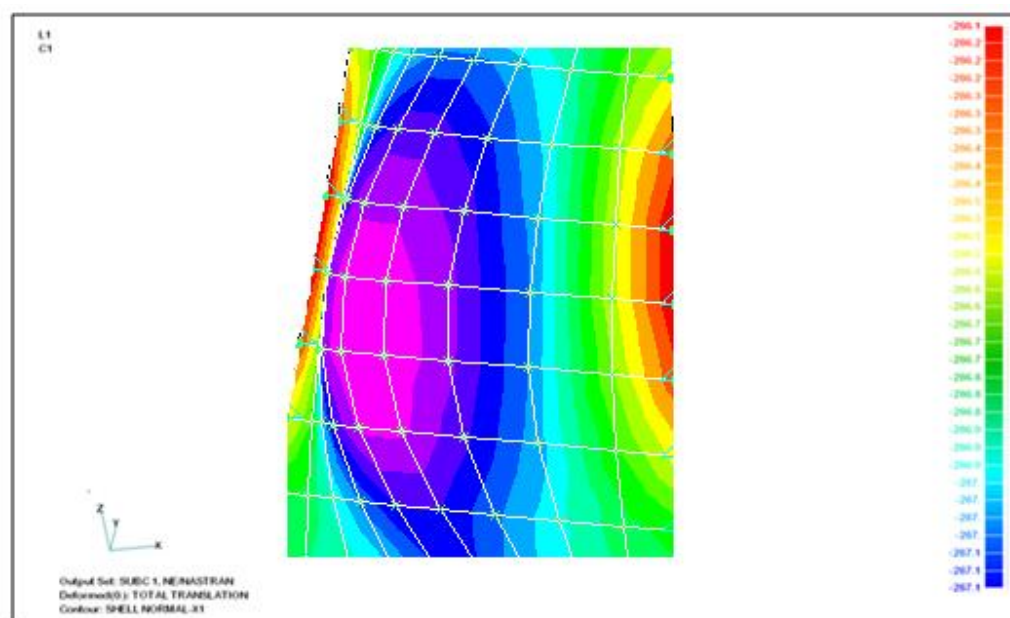**Figure (6). First mode shapes of the gate of the dike .**

Figure (7) . Second mode shapes of the gate of the dike .
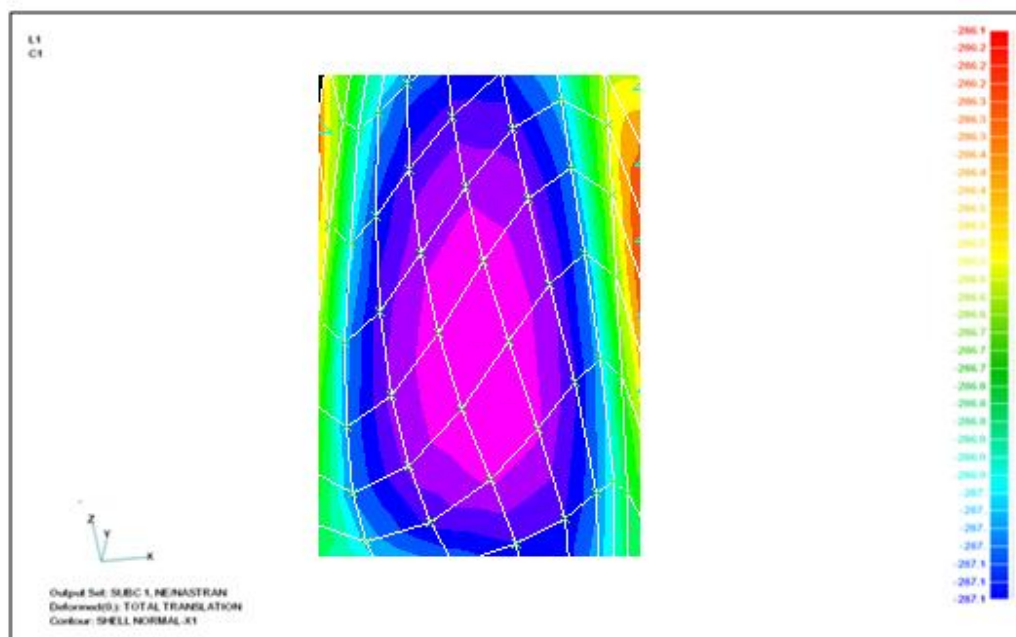
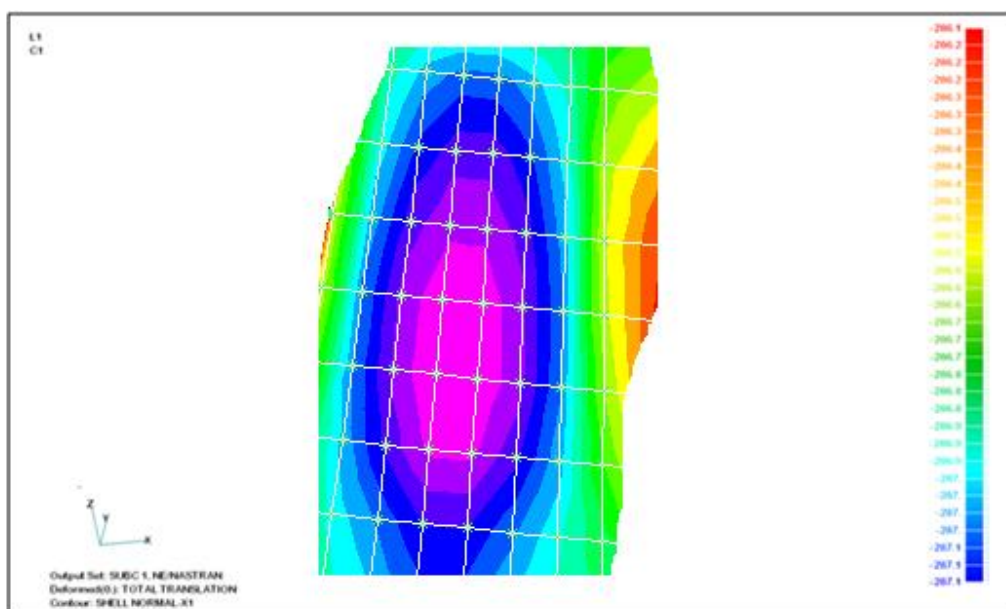**Figure (8). Third mode shapes of the gate of the dike .**

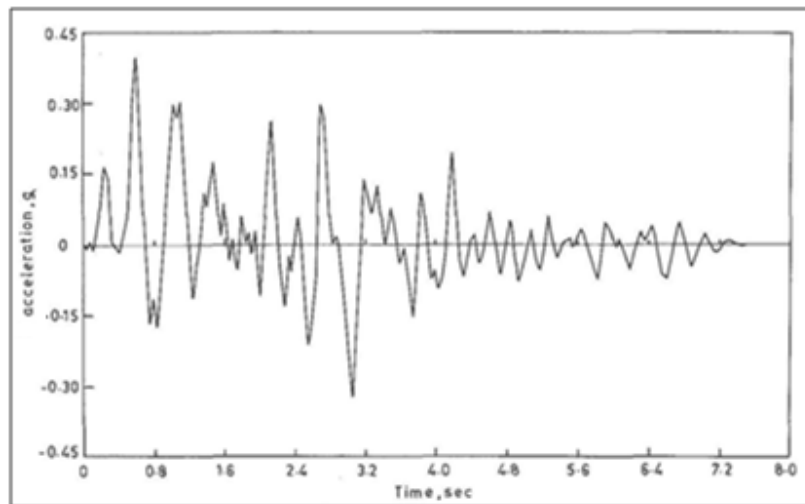**Figure (9). Fourth mode shapes of the gate of the dike.**

Figure (10). Displacement variance of critical excitation.

4. Summary

This study outlines a method to obtain the variance of the dike's gate at the critical random excitation for a given linear system. For purposes of application in engineering, the input is taken as an unknown nonstationary process modulated by a known enveloping function. The mean square value of the random process is required to be known. A frequency domain solution is presented for finding the critical power spectral density function of the nonstationary random input. The procedure is illustrated with the example of a gate of a dike, it is fairly obvious that the critical power spectral density function should peak near the resonant- frequency. However, with heavily damped systems and with multi degree systems, the structure of the input power spectral density function is less obvious. The numerical results obtained show that the sense of criticality is not too severe both in the input and in the response variance. Thus one can expect realistic peak excitation and peak responses from the present solution when used in the random analysis of important structures and equipment.

Further modification of the method restricts the class of allowable inputs and to minimize damage variables other than the response variance is presently under investigation which will be very useful to investigate the danger of cumulative damage in Al Mosul dike (North of Iraq).

5. References

[1] Mrzyg³ód, M., 2005," Parametrical Optimization of Structures Working in High-Cycle Load Conditions ", Cracow University of Technology, PhD Thesis.

[2] Burton, T.D. , 1994," Introduction to Dynamic Systems Analysis", McGraw-Hill, Inc.

[3] Billings, S. A. and Tsang, K. M., 1989,"Spectral Analysis for Non-Linear Systems", Part 1: parametric non-linear spectral analysis, Mechanical System and Signal Processing, 3(4), 319-339, doi: 10.1016/0888-3270(89)90041-1 C929

[4] Shinozuka, M., Oct. 1970,"Maximum Structural Response to Seismic Excitations" , Journal of Engineering Mechanics Division, ASCE, Vol. 96, No. EM5, Proc. Paper 7620, , pp. 729-738.

[5] Hearn, G. E., Metcalfe, A. V. & Lamb, D., 8th--10th September 2000,"All at Sea with Spectral Analysis", Proceedings of the Industrial Statistics in Action 2000 International Conference, University of Newcastle upon Tyne, ed. Coleman, S., Stewardson, D. and Fairbairn, L., Volume II, 217--235, University of Newcastle upon Tyne

[6] Ross, C. , 1995, "Differential Equations An Introduction with Mathematica", Springer-Verlag, New York Berlin Heidelberg London Paris Tokyo Hong Kong Barcelona Budapest.

[7] Bigges, J.M., 1964,"Introduction to Structural Dynamic", N.Y., McGraw-Hill.

[8] D. Luenberger,1979,"Introduction to Dynamic Systems Theory", models, and applications. John Wiley and Sons, New York Chichester Brisbane Toronto, [10] U. Nehmzow. Animal and Robot Navigation. Robotics and Autonomous Systems, 15:71-81, 1995.

[9] Wu , J.S. ,and Chou, H.M., 1999 ,"A New Approach for Determining The Natural Frequencies and Mode Shapes of a Uniform Beam Carrying Anynumber of Sprung Masses", Journal of Sound and Vibration 220, 451–468.

[10] Warburton, G.B., 1976, "The Dynamical Behaviour of Structure", 2nd Edn, Oxford Pergmon Press, P305-30.

6. Notation

The following symbols are used in this paper:

A_i, C_i = coefficients

E= variance of w (t), m^2

λ_i = system natural frequency, Hz

G = modulus of rigidity, KN/m^2

g = acceleration due to gravity

$H(x, \Omega, t)$ = frequency response function

h = impulse response function

$f_{ij}(t)$ = function of time

i,j,k = indices

J_n = Bessel's function of first kind nth order

L = Lagrangian

ℓ = height of the gate of the dike

m,n = index

$\boldsymbol{\Gamma}$ = **modal** participation factor

$\boldsymbol{\phi}_{ij}$ = orthonormal function

R(t) = envelope of response

R_w = autocorrelation functions

S (Ω) = power spectral density function

$\mathcal{U}(\mathbf{t})$ = modulating function

$\mathcal{W}(\mathbf{t})$ = Gaussian stationary random process

q(t) = input random process

$\boldsymbol{\gamma},\boldsymbol{\beta}$ = parameters in $\mathcal{U}(\mathbf{t})$

$\boldsymbol{\eta},\boldsymbol{\eta}_k$ = coefficient of viscous damping

$\boldsymbol{\psi}_{ij}$ = phase angles

$\boldsymbol{\omega}_i$ = angular frequency rad/sec

$\boldsymbol{\Pi}$ = Lagrangian multiplier

$\boldsymbol{\rho}$ = density kg/m^3

$\boldsymbol{\sigma}^2$ = variance of response

$\boldsymbol{\phi}_{ij}$ = mode shapes

$\boldsymbol{\phi}_n$ = orthonormal functions

$\boldsymbol{\tau},\boldsymbol{\tau}_1,\boldsymbol{\tau}_2$ = dummy variables

Free Vibration of Axisymmetric Thin Oblate Shells Containing Fluid

Talib H. Elaikh

Mechanical Engineering Department
College of Engineering
Thi-Qar University

Abstract

A theoretical analysis for the free , axisymmetric, vibrations of an isotropic thin oblate spheroid shell filled partially or completely with an incompressible, non-viscous, irrotational fluid is considered. The Rayleigh – Ritz's method is used to obtain an approximate solution which coincides with the exact solution for the cases of an empty or completely filled shell.

The vibration of the shell is examined using the non – shallow shell theory. The analysis is based on considering the oblate spheroid as a continuous system constructed from two spherical shell elements matched at the continuous boundaries. Solutions are presented to show the effect of the angle of filling fluid on the shell natural frequencies. The effect of shell geometric parameters on the frequencies is also investigated. Natural frequencies are calculated for the shell in both empty and filled cases. It was found that their frequencies are decreased with the increase of fluid level in the shell. The analytical solution is compared with available test results. Good agreement is shown between test results found in the literature and predicted natural frequencies.

Keywords: Oblate spheroid, thin shells, axisymmetric spheroid, incompressible fluid.

الاهتزازات الحرة للقشريات المتناظرة المحور نحيفة الجدران شبه البيضوية الشكل المحتوية على مائع

المستخلص

يتناول هدا البحث تحليلاً نظرياً للاهتزازات الحرة للقشريات نحيفة الجدران شبه البيضوية الشكل المتناظرة المحور والمتشابهة الخواص في جميع الاتجاهات والممتلئة جزئياً أو كلياً بمائع ساكن ، عديم اللزوجة وغير قابل للانضغاط. وقد استخدمت طريقة (Rayliegh – Ritz) للحصول على الحل التقريبي والذي يطابق الحل الدقيق لحالات القشرية الفارغة والمملوءة بالكامل.

وقد تم استخدام (نظرية القشريات العميقة) لاختبار اهتزازات القشرية. وتعتمد هذه التقنية على أساس القشرية شبه البيضوية كمنظومة مستمرة مركبة من قشريتين نصف كرويتين متناظرتين على طول حدودها المستمرة.

تم عرض الحلول لبيان تأثير زاوية الإملاء للمائع على الترددات الطبيعية للقشرية. تم احتساب الترددات الطبيعية للقشرية في حالتيها الفارغة والمملوءة ووجد بان هده الترددات تقل بزيادة مستوى السائل داخل القشرية. وقورنت نتائج التحليل النظري مع النتائج المتيسرة للبحوث ذات العلاقة حيث أظهرت تطابقاً جيداً.

1. Introduction

Dynamic characteristics of oblate spheroidal shell filled with fluid are of great important in a variety of engineering applications ,such as, vibration of liquid oxygen tanks which are important components in upper stages space vehicles, and many other engineering and industrial systems. To show the resonance problem which is considered one of the important dynamic problems which results from these applications, free vibration of this type of shells are studied.

Although numerous papers have been written on the free vibration of oblate spheroidal shell, no work appears to have been done on the problem of fluid- filled isotropic oblate spheroidal shell. Nevertheless, there exists many papers in the case of spherical shell filled with fluid. Hoppmann[1]. Discussed both free and forced vibrations of a thin elastic orthotropic spherical shell, which is the general case of Love's spherical shell problem. Penzez and Burgin [2]. Discussed the problem of free vibration of thin isotropic oblate spheroid shell, Galerkin's method was employed. The effect of bending on vibration of spherical shell was reported by Kalinin's [3]. AL-Jumaily and Najim [4] considered the free vibration characteristics of an oblate spheroidal shell. They used Rayleigh variation method to obtain the natural frequencies and mode shape. Natural frequencies of an elastic

hemispherical shell filled with a liquid and subjected to axisymmetric vibrations has been formulated by Tai and Wing [5]. The general non-axisymmetric free vibration of an isotropic elastic spherical shell filled with a compressible fluid medium is investigated by Chen and Ding [6]. Hayak & Dimaggio [7]. and Yen & Dimaggio [8] have considered the axisymmetric extensional motion of submerged spheroidal shell, free and forced, respectively. Engin and Lin [9] considered the free vibration of a thin, homogenous spherical shell containing fluid. The solution of vibration of a fluid-filled spherical membrane appears in Morse and Feshbach [10].Recently, free vibration of a thin spherical shell filled with a compressible fluid is investigated by Mingsian & Kuonung [11].

This study was undertaken to examine the effect of fluid filled on the vibration of thin oblate spheroidal shells. The comparison was made between the shell in cases of empty and filled with incompressible fluid like water. From the results, the changes of the natural frequencies of the mode of vibration will occur. Rayleigh – Ritz's method will be used to investigate the free vibration characteristics of this type of shells.

2. Equations of motion

The theoretical model in this paper consists of a thin elastic oblate spheroid shell under free, axisymmetric, non-torsional vibration filled with incompressible fluid. The analysis based on a non-shallow shell theory and Rayleigh-Ritz method to derive the equation of motion and then obtain the natural frequencies in cases of empty and filled shells.

2.1. Formulation of the problem

From the geometry shown in Figure (1) ,an oblate spheroidal shell is modeled as a structure composed of two spherical shells joined rigidly at their ends. Centers of curvature of their elements fall along the minor axis of the proposed structure. The radius of curvature at the apex of the shell (R_r) can be obtained from the geometrical formulation [2] :

$$R_\Phi = \frac{a(1-e^2)}{(1-e^2\cos^2\Phi')^{3/2}} \tag{1}$$

Setting (Φ') to zero results the radius of the shell at the apex as:

$$R_r = \frac{a}{(1-e^2)^{1/2}} \tag{2}$$

where,

$$e = \left[1 - \frac{b^2}{a^2}\right]^{\frac{1}{2}} \tag{3}$$

$e = 0$ for sphere   , $e = 1$ for plate.

An approximate opening angle (Φ_0) may be obtained by using the following formula:

$$\Phi_o = \cos^{-1}\frac{R_r - b}{R_r} \tag{4}$$

Assuming that the temporal and spatail dependence of the free vibration are separable, the transverse displacement and the tangentail displacement may be assumed as [4]:

$$w(\Phi, t) = W(\Phi) . \cos wt$$

$$u_\Phi(\Phi, t) = U_\Phi (\Phi) . \cos wt \tag{5}$$

Where (w) denotes the circular frequency, t: time and Φ denotes the angle measured from the (vertical axis). The actual Φ - dependent coefficient of the varaible was derived in Kalanins [3], as follows:

$$W(\Phi) = \sum_{i=1}^{3}(A_i P_{ni}(x) + B_i Q_{ni}(x)), \quad U_f(\Phi) = \sum_{i=1}^{3} -(1+n)D_i\left[A_i P'_{ni}(x) + B_i Q'_{ni}(x)\right] \tag{6}$$

Where

$$D_i = \frac{1+(1_i - 2)/[(1+n)(1+x)]}{1-n-1_i + x(1-n^2)\Omega^2/(1+x)} \ , \ n_i = -0.5 + \sqrt{0.25 + 1_i} \ ,$$

$$x = 12R_r^2/h^2, \quad x = \cos \Phi \tag{7}$$

The parameters $1_i's$ are the roots of the cubic equation :

$$I^3 - \left[4 + (1-n^2)\Omega^2\right]I^2 + \left[4 + (1-n)(1-n^2)\Omega^2 + (1+x)(1-n^2)(1-\Omega^2)\right]I +$$
$$(1-n)(1-n^2)\left[\Omega^2 - 2/(1-n)\right]\left[1 + x(1+n)(\Omega^2 + 1/(1+n))\right] = 0 \tag{8}$$

The non-dimensional frequency is defined as:
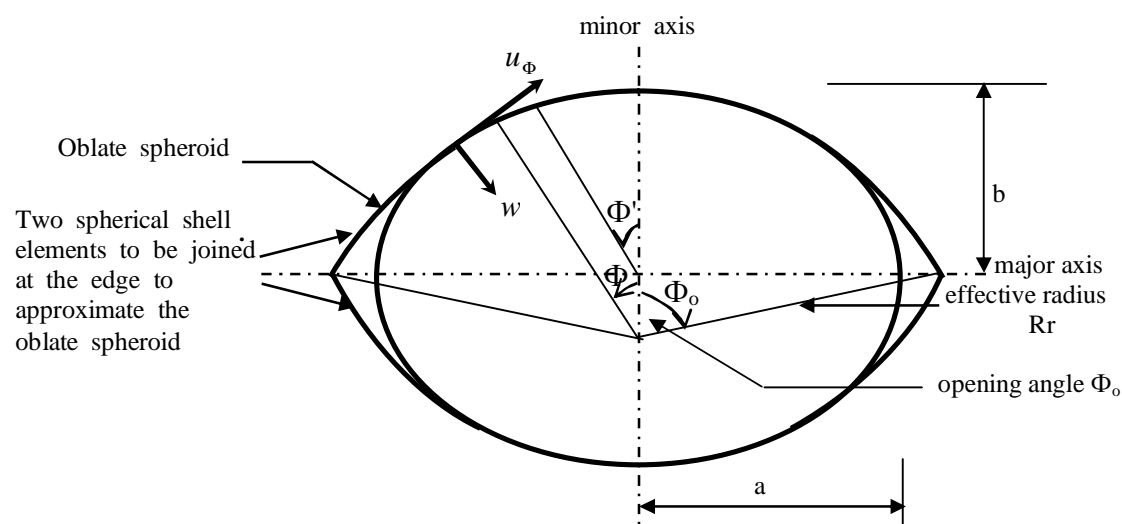
$$\Omega^2 = rw^2 R_r^2 / E \tag{9}$$

Figure (1). An oblate spheroid and its approximate of two spherical shell elements joined at the edge.

2.2 Energy method

Because of the complexity encountered in solving the exact equation of motion of an oblate spheroidal shell, an approximate energy approach based on Rayleigh-Ritz's method is used. Rayleigh-Ritz's method is an extension of Rayleigh's quotient which can be used for more complex elastic bodies and helps to determine the natural frequencies and their associated mode shapes with general boundary conditions in an approximate form. In order

to apply Rayleigh method, and its extension, the Rayleigh-Ritz's procedure, we need to derive expression for the maximum kinetic and potential energies. Physically, the frequency oscillation is found from the ratio of these energies [12].

The kinetic energy of the system is defined to be:

$$T = T_s + T_f \tag{10}$$

Where the kinetic energy T_S of an oblate spheroidal shell is:

$$T_S = \int_{-h/2}^{h/2} \int_0^{2p} \int_0^{2p} \tfrac{1}{2}\, r \left[\left[u^{\bullet}_f \right]^2 + \left[w^{\bullet} \right]^2 \right] R_{\Phi}\, R_q \sin\Phi' d\Phi' dq\ dz \tag{11}$$

And the kinetic energy T_f of incompressible ,non-viscous, irrotational fluid is given by:

$$T_f = 2\int_0^r \int_0^{2p} \int_0^a\, r_{\ f} \left[w^{\bullet} \right]^2 R_{\Phi}\, R_q \sin\Phi' d\Phi' da\ dr \tag{12}$$

The dot indicates a time derivative.

The strain energy of the shell is given by [13]:

$$U = \int_{-h/2}^{h/2} \int_0^{2p} \int_0^{2p} \tfrac{1}{2} [\text{Б}_{\Phi'}\ \text{Є}'_{\Phi'} + \text{Б}_{\theta}\, \text{Є}\,'_{\theta}]\ R_{\Phi}\ R_{\theta} \sin\Phi'\ d\Phi\ d\theta\ dz \tag{13}$$

The stress in terms of strain are defined as [13]:

$$\text{Б}_{\Phi'} = \frac{E}{(1-v^2)} [\ \text{Є}'_{\Phi'} + \upsilon\, \text{Є}'_{\theta}\ ]\ , \quad \text{Б}_{\theta} = \frac{E}{(1-v^2)} [\ \text{Є}'_{\theta} + \upsilon\, \text{Є}'_{\Phi'}\ ]$$

and

$$\text{Є}'_{\Phi'} = \text{Є}^{\circ}_{\ \Phi} + Z\, K_{\Phi} \qquad\qquad , \quad \text{Є}'_{\theta} = \text{Є}^{\circ}_{\ \theta} + Z\, K_{\theta} \tag{14}$$

$$\mathcal{E}^{\circ}{}_{\theta} = \frac{1}{R_q}\left[u_f \cot f' + w\right] \quad , \quad \mathcal{E}^{\circ}{}_{\Phi} = \frac{1}{R_f}\left[\frac{\partial u_f}{\partial f'} + w\right]$$

$$\mathrm{K}_{\theta} = \frac{\cot f'}{R_f{}^2}\left[(u_f - \frac{\partial w}{\partial f'})\right] \quad , \quad \mathrm{K}_{\Phi} = \frac{1}{R_f}\cdot\frac{\partial}{\partial f'}\left[\frac{1}{R_f}(u_f - \frac{\partial w}{\partial f'})\right] \tag{15}$$

At the natural frequency (ω), and assuming separation of variables, the shell displacements may be written in the following forms [13].

$$w(\Phi', t) = W(\Phi') \cdot e^{\,i\omega t}$$

and $$\tag{16}$$

$$u_{\Phi}(\Phi', t) = U_{\Phi}(\Phi') \cdot e^{\,i\omega t}$$

Taking e^{iwt} in Eqs. (16) to be unity and integrating the equations (11) and (12) with respect to (z) and (r), respectively, the maximum kinetic energy of the system will take the form:

$$\mathrm{T}_{max} = \frac{w^2\, r\, h}{2}\int_0^{2p}\int_0^{2p}(U_{\Phi}{}^2 + W^2)\,R_{\Phi}\,R_{\theta}\,\sin\Phi'\,d\Phi'\,d\theta +$$

$$2rw^2\,r_f\int_0^{2p}\int_0^{a}(W^2)\,R_{\Phi}\,R_{\theta}\,\sin\Phi'\,d\Phi'\,d\,a \tag{17}$$

Where $\quad r = R_r \quad$ and $\quad R_q = \dfrac{a}{(1 - e^2\cos^2\Phi')^{1/2}}$

Substituting equations (14) , (15) and (16) in equation (13), the maximum strain energy of the shell is obtained after performing the integration with respect to (z) and taken e^{iwt} to be unity:

$$U_{max} = \frac{Eh}{2(1-u^2)} \int_0^{2p} \int_0^{2p} \left\{ \frac{h^2}{12} \left[\frac{1}{R_\Phi^2} \left[\frac{\partial}{\partial \Phi'} \left[\frac{U_\Phi}{R_\Phi} - \frac{\partial W}{R_\Phi \partial \Phi'} \right] \right] \right]^2 \right.$$

$$+ \frac{\cos^2 \Phi'}{R_\phi^2 R_q^2 \sin^2 \Phi'} \left[U_\Phi - \frac{\partial W}{\partial \Phi'} \right]^2 + 2u \frac{\cos \Phi'}{R_q R_\Phi^2 \sin \Phi'} \left[U_\Phi - \frac{\partial W}{\partial \Phi'} \right].$$

$$\cdot \frac{\partial}{\partial \Phi'} \left[\frac{U_\Phi}{R_\Phi} - \frac{\partial W}{R_\Phi \partial \Phi'} \right] \right] + \frac{1}{R_\Phi^2} \left[\frac{\partial U_\Phi}{\partial \Phi'} + W \right]^2 \qquad (18)$$

$$+ \frac{1}{(R_q \sin \Phi')^2} (U_\Phi \cos \Phi' + W \sin \Phi')^2$$

$$+ \frac{2u}{R_q R_\Phi \sin \Phi'} \left[\frac{\partial U_\Phi}{\partial \Phi'} + W \right].(U_\Phi \cos \Phi' + W \sin \Phi') \left. \right\}.$$

$$R_\Phi R_q \sin \Phi' d\Phi' dq$$

3. Frequency equation

For a system with no dissipation losses, as those due to friction or damping, the maximum potential energy equals the maximum kinetic energy, i. e.

$$U_{max} = T_{max} \qquad (19)$$

The kinetic energy for $\omega=1$ rad/sec is customarily define as T^*_{max} and, therefore,

$$T_{max} = \omega T^*_{max} \qquad (20)$$

An expression for the natural frequency may be written as :

$$W_i^2 = \frac{U_{max}}{T^*_{max}} \qquad i = 1, 2, 3, ..., n \qquad (21)$$

Following the procedure of Rayleigh – Ritz's method, the radial (or transverse) and tangential displacements can be written in power series form as :

$$w(\Phi') = \sum_{i=1}^n a_i . W_i(\Phi') , \quad u_\Phi(\Phi') = \sum_{i=1}^n b_i . U_{\Phi i}(\Phi') \qquad (22)$$

where a_i and b_i are coefficients to be determined. The functions $w(\Phi')$, $u_\Phi(\Phi')$ satisfy all the geometry boundary conditions of the system. Equation (21) is an exact expression for the frequency according to Rayleigh quotient. In order to use the procedure of Rayleigh – Ritz's method, equation (22) is substituted into equation (17) and (18), then the results are used in equation (21). After some mathematical manipulations, the following equation will result:

$$w_i^2 = \frac{U_{max}}{T^*_{max}} = \frac{\sum_{i=1}^{n}\sum_{j=1}^{n} c_i\, c_j\, k_{ij}}{\sum_{i=1}^{n}\sum_{j=1}^{n} c_i\, c_j m_{ij}} \qquad \text{i = 1, 2, 3, ..., n} \qquad (23)$$

where,

$$U_{max} = \sum_{i=1}^{n}\sum_{j=1}^{n} c_i\, c_j\, \frac{Ehp}{(1-u^2)} \int_0^{2p} \{ \frac{h^2}{12R_\Phi^4}\left[U'_{\Phi i}\, U_{\Phi j}{}' - 2U_{\Phi i}{}'\, W_i{}'' + W_i{}''\, W_j{}''\right]\sin\Phi'$$

$$+ \frac{u\, h^2}{6R_q\, R_\Phi^3}\left[U_{\Phi i}\, U_{\Phi i}{}' - U_{\Phi i}\, W_i{}'' - U_{\Phi i}{}'\, W_i{}' + W_i{}'\, W_i{}''\right]\cos\Phi'$$

$$+ \frac{h^2}{12R_\Phi^2\, R_q^2}\left[U_{\Phi i}U_{\Phi j} - 2U_{\Phi i}\, W_i{}' + W_i{}'\, W_j{}'\right]\frac{\cos^2\Phi'}{\sin\Phi'}$$

$$+ \frac{1}{R_\Phi^2}\left[U_{\Phi i}{}'\, U_{\Phi j}{}' + 2U_{\Phi i}{}'\, W_i + W_i\, W_j\right]\sin\Phi' \qquad (24)$$

$$+ \frac{1}{R_q^2}\left[U_{\Phi i}\, U_{\Phi j}\, \frac{\cos^2\Phi'}{\sin\Phi'} + 2U_{\Phi i}\, W_i\cos\Phi' + W_i\, W_j\sin\Phi' \right]$$

$$+ \frac{2u}{R_\Phi\, R_q}\left[U_{\Phi i}\, U_{\Phi i}{}'\, \cos\Phi' + U_{\Phi i}{}'\, W_i\sin\Phi' + U_{\Phi i}\, W_i\cos\Phi' + W_i\, W_i\sin\Phi' \right] \}.$$

$$. R_\Phi\, R_q\, d\Phi'$$

and

$$T^*_{max} = \sum_{i=1}^{n}\sum_{j=1}^{n} c_i\, c_j \int_0^{2p} r\, hp\left[U_i\, U_j + W_i\, W_j\right] R_\Phi\, R_q\, \sin\Phi'\, d\Phi' +$$

$$\sum_{i=1}^{n}\sum_{j=1}^{n} c_i\, c_j \int_0^{2p} 2rr_f\, a\,(W_i\, W_j)\, R_\Phi\, R_q\, \sin\Phi'\, d\Phi' \qquad . \qquad (25)$$

Equations(24) and (25) gives the physical properties of the shell from the stiffness and mass distribution point of view. The stiffness and mass of the shell are given by the following two equations respectively:

$$
\begin{aligned}
k_{ij} = \frac{Ehp}{(1-u^2)} \int_0^{2p} \Big\{ & \frac{h^2}{12R_\Phi^4} \big[U_{\Phi i}{}'\ U_{\Phi j}{}' - 2U_{\Phi i}{}'\,W_i{}'' + W_i{}''\,W_j{}'' \big] \sin\Phi' \\
& + \frac{u\,h^2}{6R_q\,R_\Phi^3} \big[U_{\Phi i}\,U_{\Phi i}{}' - U_{\Phi i}\,W_i{}'' - U_{\Phi i}{}'\,W_i{}' + W_i{}'\,W_i{}'' \big] \cos\Phi' \\
& + \frac{h^2}{12R_\Phi^2\,R_q^2} \big[U_{\Phi i}\,U_{\Phi j} - 2U_{\Phi i}\,W_i{}' + W_i{}'\,W_j{}' \big] \frac{\cos^2\Phi'}{\sin\Phi'} \\
& + \frac{1}{R_\Phi^2} \big[U_{\Phi i}{}'\,U_{\Phi j}{}' + 2U_{\Phi i}{}'\,W_j + W_i\,W_j \big] \sin\Phi' \\
& + \frac{1}{R_q^2} \Big[U_{\Phi i}\,U_{\Phi j}\,\frac{\cos^2\Phi'}{\sin\Phi'} + 2U_{\Phi i}\,W_i\cos\Phi' + W_i\,W_j\sin\Phi' \Big] \\
& + \frac{2u}{R_\Phi\,R_q} \big[U_{\Phi i}\,U_{\Phi i}{}'\cos\Phi' + U_{\Phi i}{}'\,W_i\sin\Phi' + U_{\Phi i}\,W_i\cos\Phi' + W_i\,W_i\sin\Phi' \big] \Big\}. \\
& \cdot R_\Phi\,R_q\,d\Phi'
\end{aligned}
$$
(26)

and

$$
m_{ij} = \int_0^{2p} r\,hp \big[U_i\,U_j + W_i\,W_j \big] R_\Phi\,R_q\,\sin\Phi'\,d\Phi' + \int_0^{2p} 2rr_f\,a\,(W_i\,W_j)\,R_\Phi\,R_q\,\sin\Phi'\,d\Phi'
$$
(27)

In order to minimize the approximate value, which is given by equation (23), it should be differentiated with respect to c_i and equating the resulting expression to zero, that is :

$$
\frac{\partial w^2}{\partial c_i} = \frac{T_{max}^*\,\dfrac{\partial U_{max}}{\partial c_i} - U_{max}\,\dfrac{\partial T_{max}^*}{\partial c_i}}{T_{max}^{*\,2}} = 0 \qquad i=1,2,3\ \dots\dots\dots n
$$
(28)

This equation can be satisfied if and only if the numerator equal zero, since $T^*{}_{max}$ is never equal to zero. The numerator can be written in a more useful form as:

$$\frac{\partial U_{max}}{\partial c_i} - \frac{U_{max}}{T^*_{max}} \frac{\partial T^*_{max}}{\partial c_i} = 0 \qquad \text{i = 1, 2, 3, ..., n} \qquad (29)$$

It is as given by equation (21), $w_i = \dfrac{U_{max}}{T^* max}$, and n is the number of terms in the approximate solution. The infinite degrees of freedom system has been replaced by an n degrees of freedom system. Therefore, Equation (28) can be written in general matrix notation as :

$$\left[\{K\} - w^2\{M\}\right]\{c\} = \{0\} \qquad (30)$$

The stiffness and mass are matrices determined at the edge ($\Phi = \Phi_o$) of the sphereical shell using (Eqs. 26, 27) respectively, which resulted values substituted in the following determinant:

$$\begin{vmatrix} k_{11} - \Omega^2 m_{11} & k_{12} - \Omega^2 m_{12} & k_{13} - \Omega^2 m_{13} \\ k_{21} - \Omega^2 m_{21} & k_{22} - \Omega^2 m_{22} & k_{23} - \Omega^2 m_{23} \\ k_{31} - \Omega^2 m_{31} & k_{31} - \Omega^2 m_{32} & k_{33} - \Omega^2 m_{33} \end{vmatrix} = 0 \qquad (31)$$

4. Calculation of natural frequency

The calculation of the natural frequency is carried out by specifying an intial guess then evaluting the determiniant of equation (31). Increasing the frequency by small increments and repeating the same procedure until the value of the determinant changes in sign. This indicates that a natural frequency has a new value. The frequency increment is then minimized and the operation is repeated until the desired accuracy of the non-dimentional natural frequency is obtained when the determinant is vanished.

In case of zero filling angle (a) in equations (17) ,natural frequencies for an empty shell can be calculated using the same procedure of Rayleigh –Ritz method.

5. Results and discussion

Calculations to test the theory in the case of partially or completely filled shells are presented herein. The parameters used in this study are: a=0.185 mm, h=0.0015mm, $n = 0.3$, $E = 68 GN/m^2$, e = 0.683, $r_s = 2720 kg/m^3$, and $r_f = 1000 kg/m^3$. The parameters used here for the empty shell are the same as in refrence[4].

For validity purposes, a comparison is made between the theoretical results obtained by Rayleigy-Ritz method (RRM) in this paper and the boundary maching method (BMM) in AL-Jumaily and Najim [4] with some experimental results which are taken from AL-Jumaily and Najim [4] for the case of filling angle ($a = 0$). There is an excellent coincidence between the theoretical results of RRM and BMM method. However, the theoretical results obtained by RRM are higher than experimental results, because the theoretical spherical caps are in general stiffer than the corresponding experimental oblate spherical shells.. See Table (1).

**Table (1) . Theoretical and experimental natural frequencies in Hz
of thin oblate spheroidal shell (α = 0) .**

Frequency	BMM[4]	RRM (Preset work)	Experimental [4]
1	2500	2520	2400
2	2978	2973	2600
3	3082	3090	2900
4	3180	3190	3100

Figures (1) and (2) show the non-dimensional natural frequencies ($I = \sqrt{E/r}.w.a$) of the first two modes of vibration as functions of the eccentricity ratio of empty and filled shells by the Rayleigh- Ritz method using the non-shallow shell theory. These figures show that when the eccentricity increases, the natural frequency decreases, whereas that of an empty shell is higher than those of filled shell with incompressible fluid. This drop-off in natural frequencies can be clearly justified according to the increase in the fluid induced mass.
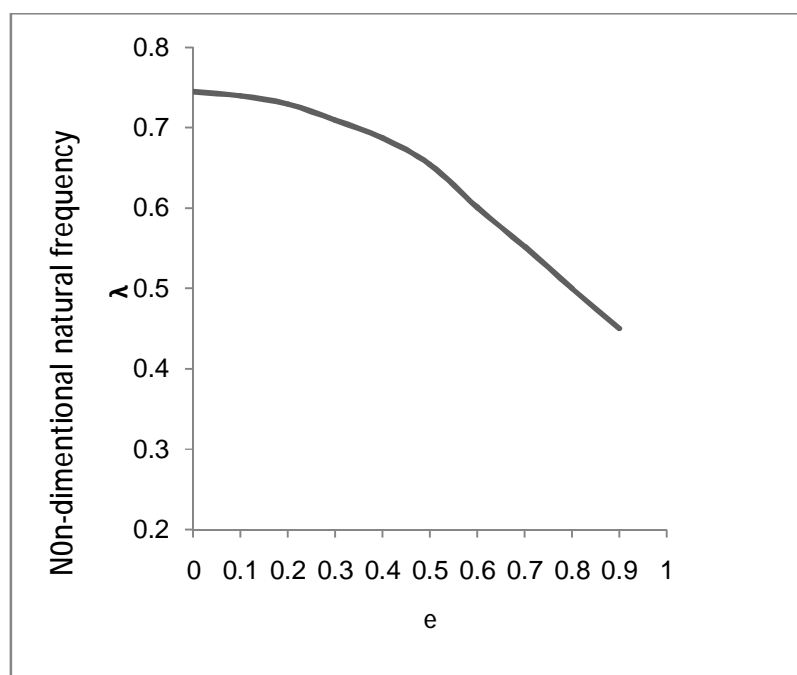
Figure (1) . Effect of eccentricity onthe first bending modes for zero filling angle .
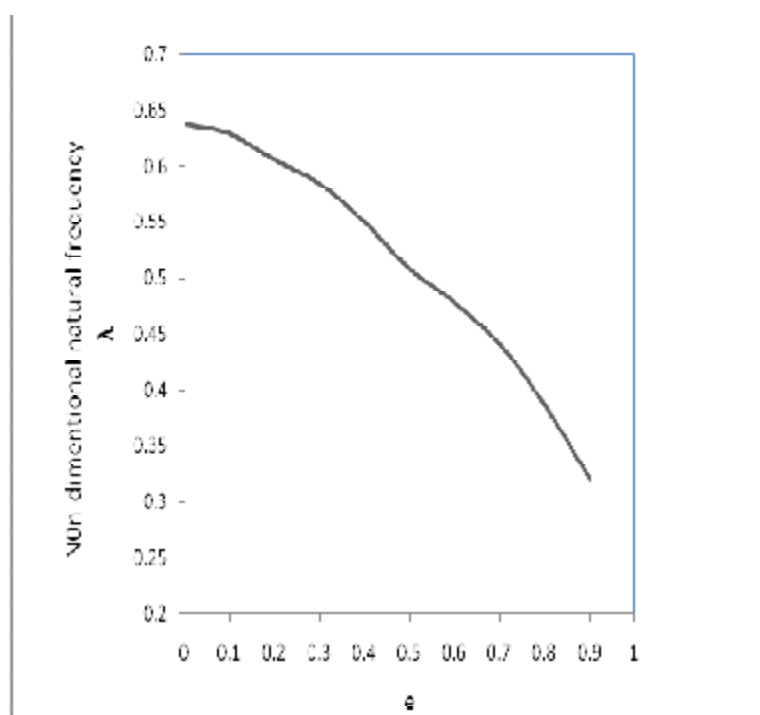

Figure (2) . Effect of eccentricity onthe first bending modes for fluid filling shells .

The free vibrations of the shell is absolutely affected by the fluid mass and thus the wet angle parameter a plays a main role in this study. The angle of filling , a , takes the values $a = 0,60,120,180,240,300,360^\circ$ and the corresponding   natural frequencies   were   computed. Figure (3) shows the decrease in the natural frequency when the fluid level in the shell increased.
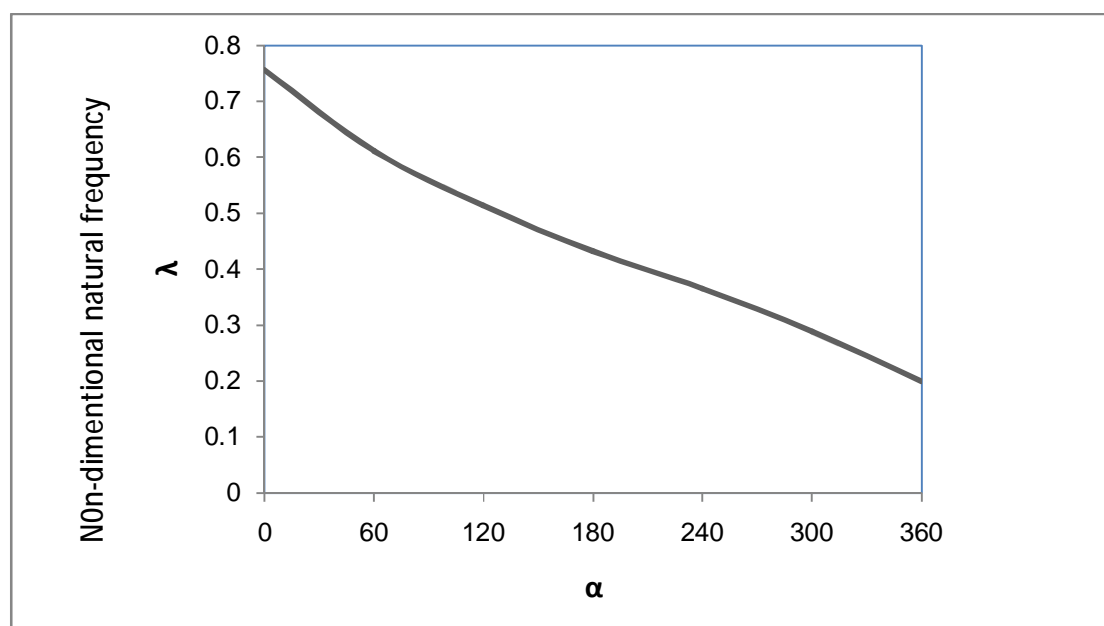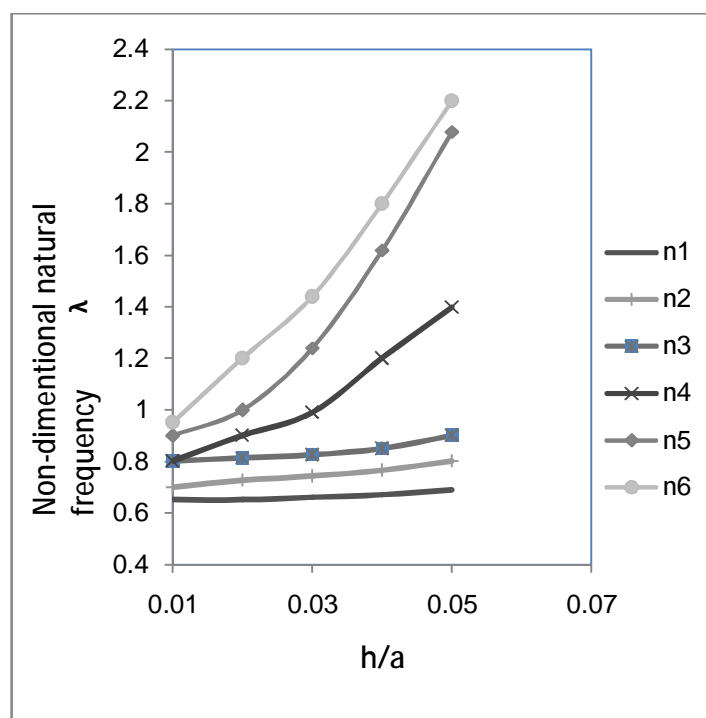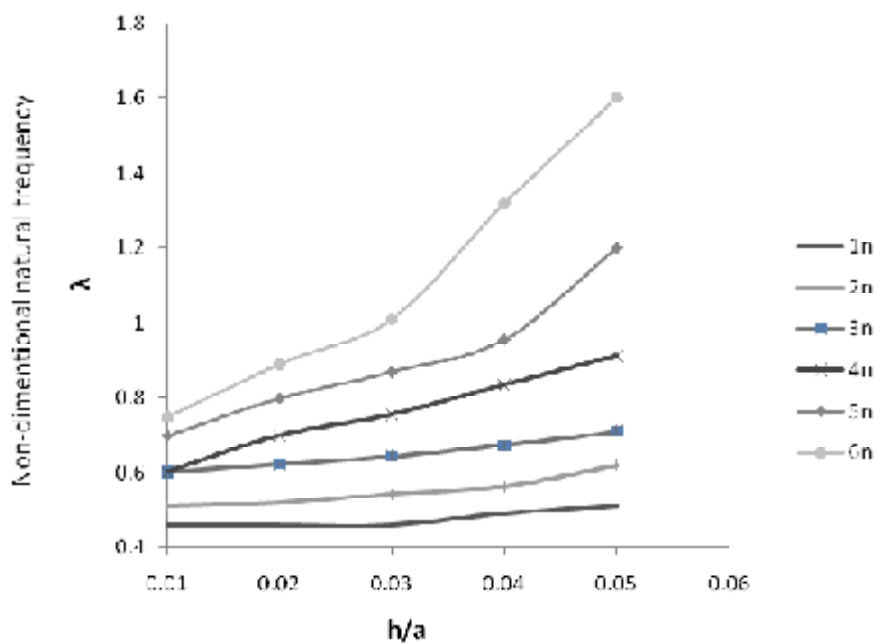

Figure (3). Variation of the non-dimentional natural frequency
of the oblate spheroid shell varies angle of filling.

The effect of the shell thickness on the free vibration characteristics of the empty and filled shell is investigated in Figs. (4) and (5). It can be noted that the variation of the natural frequency of the bending modes increases with increases of thickness ratio. This phenomena can be elaborated due to the fact that the strain energy increased with increasing the thickness ratio.
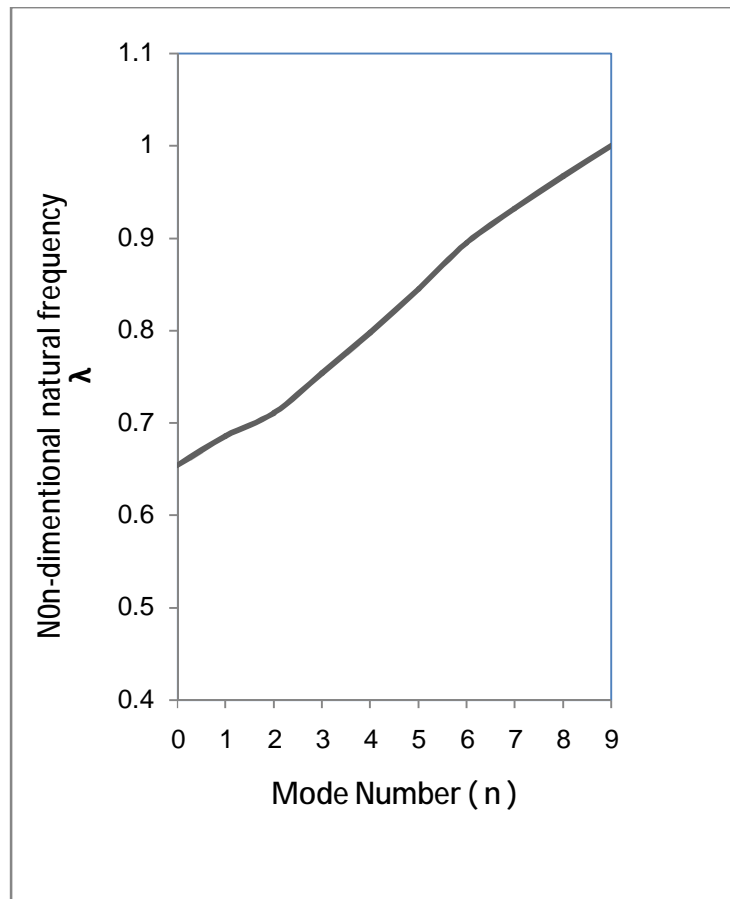
Figure(4) . Effect of the thickness ratio on the natural frequency of the oblate spheroid shell (e= 0.6, α = 0) .
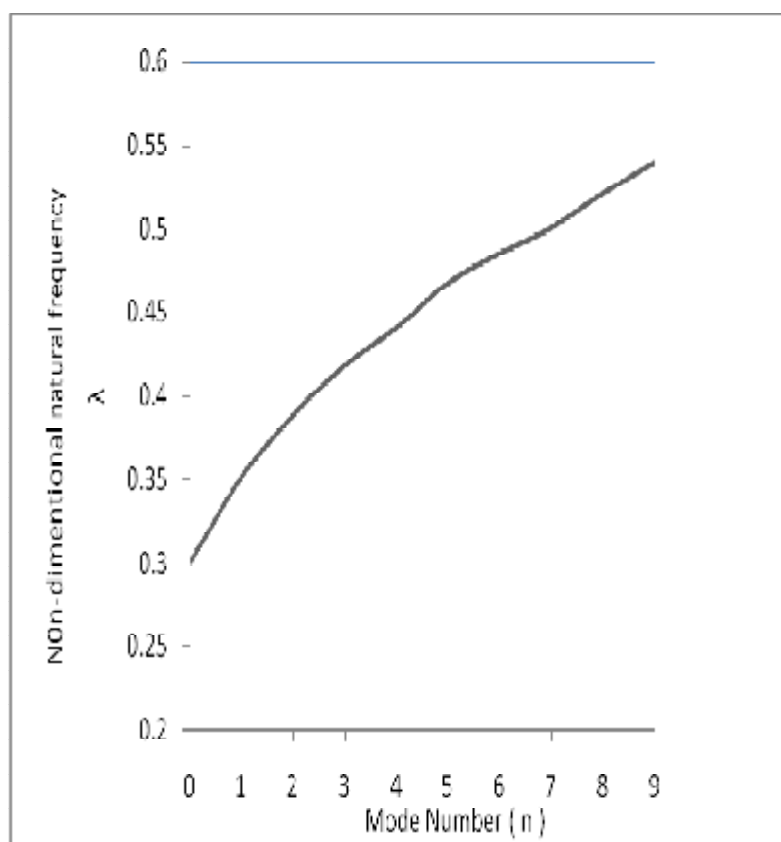

Figure(5) . Effect of the thickness ratio on the natural frequency of the oblate spheroid shell (fluid filled ,e= 0.6) .

For a different mode number (n), it is seen that as (n) increases, the natural frequency increases too. It is found that the presence of fluid decreases the natural frequency, and this can be explained as the system-mass increases, as shown in Figures (6) and(7).

Figure(6) . Variation of the non-dimentional natural frequency of the oblate spheroid shell varies mode number of empty shell   (e = 0.6).

Figure(7) . Variation of the non-dimentional natural frequency of the oblate spheroid shell varies mode number of filled shell   (e = 0.6).

6. Conclutions

Free axisymmetric vibrations of thin isotropic oblate spheroidal shell containing incompressible fluid has been studied, to show the effect of fluid on its dynamic characteristics using non-shallow shell theory and Rayleigh-Ritz method .Numerical analysis resulted the following conclusion:

1- The kinetic energy of the system increases with the consequence that natural frequencies decrease, as can be seen from the Rayleigh-Ritz method.

2- The natural frequencies of the fluid-filled oblate shell are lower than those of the empty shell parameters of the oblate spherical itself, i.e. the fluid has effects on the frequencies. This result affects engineering design.

79

3- The analytical approach used in this paper is relativly simple and doesn't need advanced computer system, thus, it can be implementry in many engineering applications such as tank's design.

4- The resultes show the resonance frequencies of the fluid filled shell decreased with the increase of fluid level in the shell.

7.   References

[1] Hoppmann, W. H.,II and Baker, W. E., 1961," Extensional Vibrations of Elastic Orthotropic Spherical Shells", J. of Applied Mechanics, Vol. 28, pp. 229-237.

[2] Penzes, L. and Burgin, G., 1965," Free Vibrations of Thin Isotropic Oblate Spheroidal Shells", General Dynamic Report No. GD/C–BTD, 65 – 113.

[3] Kalnins ,A., 1964,"Effect of Bending on Vibrations of Spherical Shells", J. Acoust. Soc. Amer., Vol. 36 (1), PP. 74 – 81.

[4] AL-Jumaily , A.M. and Najim, F. M., 1997,"An Approximation to The Vibration of Oblate Spheroidal Shells", Journal of sound andvibration, 204(3),pp. 561-574.

[5] Tai, C. L. and Wing, H., March1966," Longitudinal Oscillation of a Propellant Filled in Flexible Hemispherical Tank", NAA S&ID, SID .

[6] Chen, W. Q. and Ding, H. J., 1999," Natural Frequencies of a Fluid-Filled Anisotropic Spherical Shells", J. Acoust. Soc. Amer., Vol. 105(1), pp. 152-174.

[7] Hayek ,S. and DiMaggio, F. L., 1965," Axisymmetric Vibration of Submerged Spheroidal Shells", Columbia Univ. Tech. Rep. No. 4, Contr. Norm. 266(67).

[8] Yen, T. and DiMaggio, F. L., 1967," Forced Vibration of Submerged Spheroidal Shells", J. Acoustic. Soc. Amer. 4I, PP. 618-626.

[9] Engin, A.E. and Liu, Y. K., 1970," Axisymmetric Response of a Fluid-Filled Spherical Shell in Free Vibrations", J. Biomech. Vol. 3, pp. 11-22.

[10] Morse, P. M. and Feshbach, H., 1953," Methods of Theoretical Physics, Part II", (McGraw –Hill , New York), pp. 1489-1472.

[11] Mingsian, R. Bai and Kuonung, Wu., 1994,"Free Vibration of a Thin Spherical Shell Containing a Compressible Fluid" , J. Acoust. Soc. Amer., Vol. 95(6), pp. 3300-3310.

[12] Rao, S. S., 1995," Mechanical Vibrations", Prentice- Hill, Inc., U. S. A. .

[13] Leissa, A.W. , 1973," Vibration of Shells " NASA SP-288, U. S. Government Printing Office, Washington D. C.

8. Nomenclature

a	Major semi – axis of an oblate spheroid shell.
b	Minor semi – axis of an oblate spheroid shell.
E	Young's modulus of elasticity (GN/m^2).
e	Eccentricity ratio.
h	Shell thickness (mm).
r	Radius of spherical shell (mm)
$P_n(x)$	Legendre function of the first kind.
$P'_n(x)$	First derivative of the Legendre function of the first kind.
$P''_n(x)$	Second derivative of the Legendre function of the first kind.
R_r	Effective radius (mm)
R_Φ , R_θ	Principal radii of curvatures of an oblate spheroid.
U_Φ	Tangential displacement mode.
u_Φ	Tangential displacement of points on shell middle surface.
W	Transverse displacement mode.
w	Transverse displacement of points on shell middle surface.
$\epsilon_\Phi, \epsilon_\theta, \epsilon_r$	Strains
Φ'	Inclination angle of an oblate spheroid.
Φ	Inclination angle of a spherical shell model.
Φ_o	Opening angle of the approximate spherical shell.
λ	Non – dimensional frequency parameter $((\rho/E)^{1/2} \omega.a)$. (used for oblate spheroid shells)
θ	Angle of rotation in the meridian direction.
r_s	Density of shell(kg/m^3).
r_f	Density of fluid(kg/m^3).
a	Angle of filling .
Ω	Non – dimensional frequency parameter $((\rho/E)^{1/2} \omega.R)$. (used for spherical shells)
ω	Circular frequency (rad / sec)